universität wien

MASTERARBEIT / MASTER'S THESIS

Titel der Masterarbeit / Title of the Master's Thesis

„Development and characterization of the Ion Laser InterAction Setup (ILIAS)“

verfasst von / submitted by

Tobias Moreau, BSc

angestrebter akademischer Grad / in partial fulfilment of the requirements for the degree of

Master of Science (MSc)

Wien, 2016 / Vienna 2016

Studienkennzahl lt. Studienblatt / degree programme code as it appears on the student record sheet:	A 066 876
Studienrichtung lt. Studienblatt / degree programme as it appears on the student record sheet:	Masterstudium Physik
Betreut von / Supervisor:	Univ.-Prof. Dipl.-Ing. Dr. Robin Golser
Mitbetreut von / Co-Supervisor:	Mag. Dr. Martin Martschini

Danksagung (Acknowledgements)

Mein großer Dank gilt Robin Golser für das Ermöglichen dieser Arbeit, sein Vertrauen und seine Unterstützung.
Martin Martschini bin ich für seine hervorragende Mitbetreuung innerhalb und außerhalb des Labors während meiner Zeit bei VERA zu größtem Dank verpflichtet. Johanna Pitters gilt mein großer Dank für die Einführung in das Themengebiet, für das Vertrautmachen mit den Eigenheiten von ILIAS und die Beantwortung vieler Fragen. Ohne der von Johanna Pitters und Martin Martschini im Vorfeld geleisteten Entwicklungsarbeit wären die in dieser Arbeit präsentierten Ergebnisse nicht zustande gekommen.
Ich danke Johannes Lachner für viele fruchtbare Diskussionen und stete Hilfsbereitschaft bei anfallenden Problemen, Alfred Priller für seine Hilfsbereitschaft, für einige Lektionen zu Technik und Ionenoptik und das Korrekturlesen dieser Arbeit und Peter Steier für seine Betreuung beim Bau der Steerer und seine lehrreichen Vorlesungen über Spurenisotope.
Ich danke Jenny Feige, Magdalena Kasberger, Johannes Lachner, Martin Martschini, Johanna Pitters und Marco Ploner für viele unterhaltsame Mittagspausen, ihre Kollegialität und Freundschaft.
Mein Dank gilt Johann Lukas für die Einführung in die Kunst des Lötens und die Grundlagen des ILIAS-Steuerungssystems, sowie für Unterstützung bei elektronischen Arbeiten.
Ich danke Ewald Friedl für zahlreiche Ratschläge und Hilfestellungen bei der Planung von mechanischen Komponenten und elektronischen Schaltungen und Gabriela Obstmayer und Wolfgang Hieß für die professionelle Fertigung vieler mechanischer Bauteile.
Ich danke Helga Schmelzer-Vincro und Sigrid Lielacher für bereitwillige und kompetente Hilfestellung bei administrativen Anliegen.
Den Betreuern der Isotopen- und Kernphysikpraktika möchte ich dafür danken, dass sie ihr Wissen mit großem Engagement weitergeben und sich dafür viel Zeit für ihre Studenten nehmen und genommen haben. Sie haben maßgeblich zu meiner Entscheidung beigetragen, mich auf dieses Gebiet zu spezialisieren.

Nicht zuletzt möchte ich meinen Eltern für ihre bedingungslose Unterstützung während meiner gesamten Studienzeit und meiner Lebensgefährtin Sandra für ihre Geduld und emotionalen Rückhalt sehr herzlich danken.

Contents

1. Introduction

This master's thesis is part of a project aiming for the development of an optical filtering technique for accelerator mass spectrometry (AMS). AMS is currently the most sensitive tool available for the measurement of rare isotopes. Since isotopic ratios ranging from 10^{-12} down to 10^{-16} are dealt with, a high efficiency as well as an extreme abundance sensitivity are required [1]. Many isotopes are up to now not accessible at that level with AMS, due to background from interfering stable isobars that cannot be separated by established techniques. Some isotopes can only be measured because of convenient circumstances, like for example when the otherwise problematic isobars do not form negative ions. Others require very high beam energies and are thus only accessible with very large accelerators. The latter concerns heavier isotopes because the higher the mass of an isotope, the more beam energy is needed to distinguish isobars by energy loss in matter. It would be highly beneficial for the field to have an isobar separation technique on hand, which is applicable more or less independent from the type of facility and to most isotopes that are of interest to AMS.

Currently two approaches for such a new technique are under investigation. One is based on element separation by selective chemical reaction of the interfering isobar with an appropriate gas and was first explored by a group from Toronto [2].

The other approach uses selective neutralization by laser photodetachment and is being developed by the research group Isotope Research and Nuclear Physics from the University of Vienna for eventual application at the Vienna Environmental Research Accelerator (VERA). For that purpose a test setup called ILIAS (Ion Laser InterAction Setup) was built (Austrian Science Fund project number P 22164-N20) and is fully operational since November 2014. Its characterization and further development are subject of this thesis.

1.1. VERA and AMS

As the name suggests, accelerator mass spectrometry (AMS) combines conventional mass spectrometry, meaning mass analysis by deflection in electrostatic and magnetic fields, with particle acceleration technique, to measure low isotopic ratios. In principle any isotopes occurring in trace amounts are targeted by AMS. Most often they happen to be radioisotopes with half lives going from several 1000 years to 10 million years. Isotopes with half lives above or below that range are accessible to conventional mass spectrome-

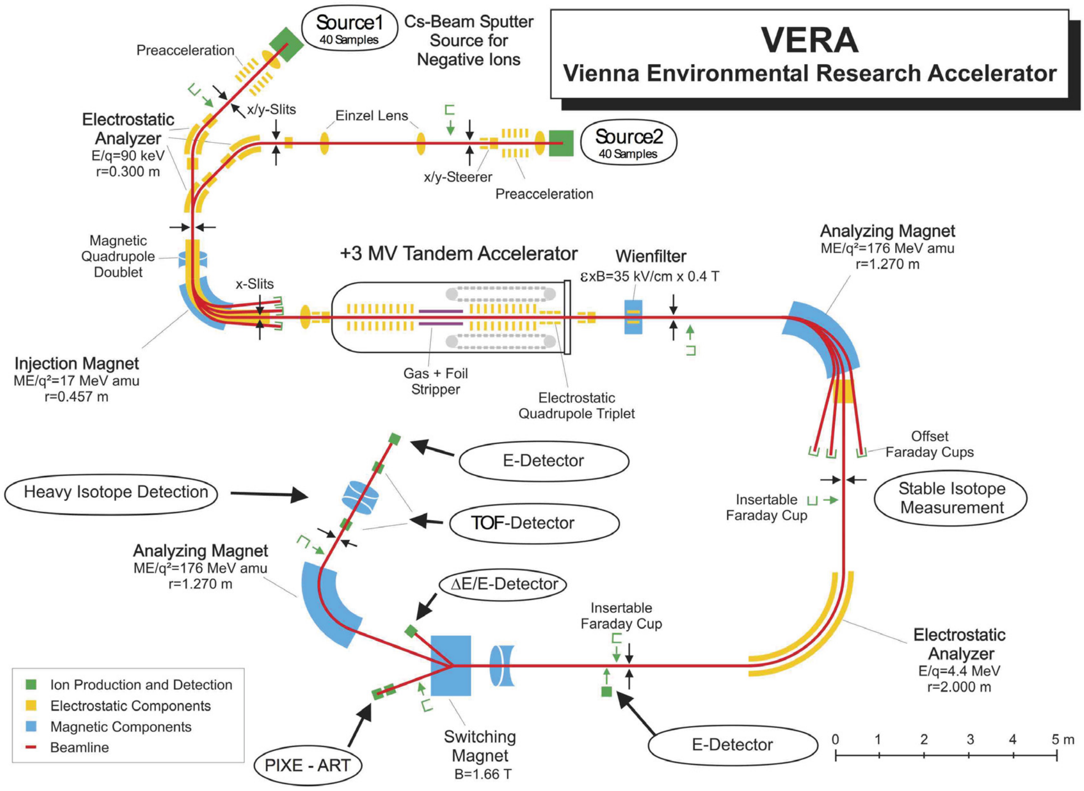

Figure 1.1.: An outline of the Vienna Environmental Research Accelerator (VERA) in early 2015. This schematic does not yet show the beamline extension of the Source2 branch that in the near future will be accomodating the laser photodetachment purification system.

try or decay counting, respectively. Applications can be found in many different areas of science, from environmental science over archeology to astrophysics (see [3] for a comprehensive review).

The Vienna Environmental Research Accelerator (VERA) is a medium sized AMS facility at the University of Vienna [4, 5]. VERA is very versatile as it is in principle suited to measure isotopes of any mass, from hydrogen to transuranic elements, and incorporates various state of the art isobar separation and identification techniques. Its structure is typical for an AMS facility of that size (figure 1.1). Two available negative ion sources are followed by a low energy mass spectrometer (electrostatic analyzer combined with an analyzing magnetic). The preselected ions then are accelerated in a tandem type accelerator, where an electrostatic voltage is exploited twice by stripping off electrons and therefore changing the charge state of the injected negative ions in a foil or gas inside the terminal at the center of the accelerator. The terminal voltage is up to 3 MV[1] and is generated by transporting charge to the accelerator terminal using a fast circulating chain of insulated metal rings (Pelletron principle). The ion energy after passing the VERA tandem accelerator can be several 10 MeV, depending on the selected charge state. A high energy mass

[1]For differently sized AMS facilities the maximum voltage can range from less than 1 MeV to 25 MeV.

spectrometer is formed by another analyzing magnet and an electrostatic analyzer. It is followed by several different detectors that can be used depending on the isotope being measured (e.g. split-anode ionization chamber, semiconductor detector, time of flight detector), as well as another analyzing magnet for the measurement of actinides. A recent review on general AMS technique can be found in e.g. [6].

As mentioned above a key to the extreme abundance sensitivity is the separation of stable and thus very abundant isobars from the extremely rare isotope of interest. This can in general be achieved by a variety of techniques. For example:

- The use of negative ions: many otherwise interfering atomic isobars of standard AMS isotopes like e.g. ^{14}C, ^{129}I and ^{26}Al have negative electron affinities and therefore cannot form negative ions in the source.
- Isobaric molecules dissociate in the stripper of the tandem accelerator or can not adopt the chosen charge state.
- In some cases (e.g. ^{10}Be, ^{36}Cl and ^{41}Ca) isobars can be separated by employing different energy loss characteristics in matter. Thereby a smaller relative difference in nuclear charge of isotope and isobar requires a higher beam energy, which restricts this method to mainly light isotopes.
- For heavy actinides (e.g. ^{236}U) usually no stable isobars exist.
- Sometimes the isotope can be injected in a molecular form, for which the molecular form of the atomic isobar is suppressed or can't be produced in the ion source.

It would be great to have available a more widely applicable technique that doesn't depend on the size of the facility. It could improve routine measurements and above all open up AMS to previously inaccessible isotopes. An example for such an isotope would be ^{182}Hf, which is of great interest for astrophysics research [7]. Its detection limit has been pushed [8], but still not enough for e.g. the search for supernova remnants on earth. It hopefully will be one of the first applications of the laser photodetachment filtering method under development for VERA.

1.2. The ILIAS project

Isobar suppression by laser photodetachment can be applied to isobaric systems where the interfering isobars have a smaller electron affinity than the isotope of interest. Using a laser with an energy in between the two electron affinities, the negative ions of the isobar can be selectively neutralized by photodetachment by overlapping the ion beam with the laser beam. This works for molecular ions as well. However, to reach a suppression efficiency

high enough for application in AMS it is necessary to lengthen the ion-laser interaction time significantly. This can be achieved in a buffer gas filled radio frequency quadrupole (RFQ) ion cooler, where the ions are radially captured in a quadrupole trapping field and thermalized by collisions with the atoms of a light gas like helium.
Such a technique is currently explored for later application at VERA. For this purpose the Ion Laser InterAction Setup (ILIAS) was built to carry out independent studies on negative ion cooling and laser photodetachment. In the near future the ion cooler and laser setup will be moved to the accelerator hall, where it will be coupled to VERA. Construction works for the additional beamline section extending the Source2 sidearm (see figure 1.1) are already ongoing and will be terminated in the months to come.

The ILIAS setup is fully operational since November 2014. A detailed description of the development work that led to the operability, as well as first characterization experiments are given in the master's thesis of Johanna Pitters [9]. The master's thesis on hand can be understood as a follow-up study, as it covers the developments and experiments that followed those described by her.
One of the main objectives was the improvement of the beam transmission through the ion cooler. This went along with the development of a novel type of beam deflector. The setup in its final state was then to be characterized with regard to transmission, buffer gas cooling and laser photodetachment capabilities, using test isotopes like ^{63}Cu and ^{127}I. Furthermore, experimental studies on the ion residence time inside the ion cooler should be carried out to get a better understanding of buffer gas cooling of high intensity negative ion beams in an RFQ.
Lastly, a first direct application for AMS was to be approached from an experimental perspective: the separation of MgO^- from AlO^- by laser photodetachment. This can be used for the measurement of ^{26}Al for which it is favorable to inject AlO^- rather than Al^- to increase the measurement efficiency.
General discussions of principles like RFQ theory and buffer gas cooling, as well as the setup description are kept rather short on purpose and will only summarize the most important aspects, since these topics were already extensively treated by Johanna Pitters.

2. Underlying principles

2.1. Isobar suppression by selective laser photodetachment

Photodetachment of an atomic or molecular negative ion (A^-) is the process where the additional electron (e^-) is detached by interaction with a photon (γ):

$$A^- + \gamma \rightarrow A + e^- \tag{2.1}$$

Photodetachment is only possible when the photon energy in the ion rest frame equals or exceeds the electron affinity of the negative ion, which is defined as the difference of the total energy of an atomic or molecular negative ion in the ground state to the total energy of the corresponding neutral atom or molecule in the ground state. It is essential to note that this process is non-resonant. There isn't a narrow resonance energy range associated with the concerned ion species in which the photon energy must fall into. It is sufficient that the photon energy exceeds the electron affinity of the anion in questions. This is very important for selective laser photodetachment as a method for isobar separation. The principle is illustrated in figure 2.1.

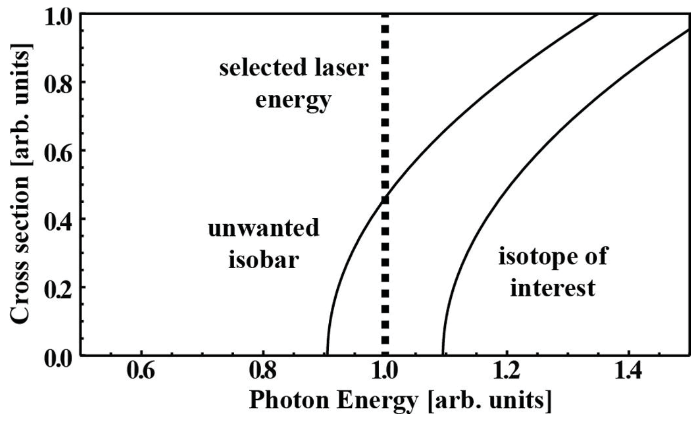

Figure 2.1.: Principle of selective laser photodetachment. Reprinted from [10], with permission from Elsevier. The shape of the photodetachment cross section near threshold actually depends on the angular momentum of the detached electron (called photoelectron) and can be described by the Wigner threshold law [11, 12]. The cross section shapes in the diagram would be characteristic for s-wave detachment.

Provided that the electron affinity of the unwanted isobar is smaller than that of the isotope of interest, the interfering isobar can be selectively neutralized by overlapping the ion

beam with a laser beam of appropriate energy. The negative ions of the isotope of interest are not affected by photodetachment because of their electron affinity being higher than the laser energy. The only prerequisite condition for the laser energy is that it must lie between the electron affinity of the isotope under investigation and the interfering isobar. This means that a laser with a certain fixed energy will most certainly be able to be used for several different isobaric systems, which is very advantageous with regard to equipment expenses. Most electron affinities roughly fall in the energy range from 0.1 eV to 3 eV. The corresponding range of laser frequencies would comprise the infrared and visible spectrum.
In some cases the electron affinity of the interfering isobar may be smaller than that of the isotope of interest. But also in such a case this method may be applicable in principle, provided molecules with more favorable properties can be used instead.

The use of laser photodetachment for isobar suppression in AMS was first explored by Berkovits et al. in the late eighties. Pioneering experiments were conducted showing the suppression of a $^{32}S^-$ beam and a $^{40}Ca^{16}O^-$ beam by a factor of 1000 [13] and later a $^{59}Co^-$ by a factor 125 [14]. Unfortunately only pulsed laser with small duty factors were available at that time and hence the reachable suppression of isobaric background was by far not enough for application in AMS.
An example for an isotope that would profit from the photodetachment separation method and will constitute a primary research objective once the setup is implemented at VERA, is ^{182}Hf [15]. By using HfF_5 the detection limit for $^{182}Hf/^{180}Hf$ could be pushed to 10^{-11}, corresponding to a suppression of the interfering isobar ^{182}W by a factor of 6000 [7]. The factor was later improved to 36000 [8]. However, this sensitivity is still too low for measurements of $^{182}Hf/^{180}Hf$ in environmental samples. This illustrates that for AMS a successful filtering method has to be able to achieve suppressions by many orders of magnitude. A self set goal for the ILIAS project is to show additional suppressions of unwanted isobars by five orders of magnitude.

Assuming a perfect laser and ion beam overlap the fraction of non-photodetached ions n/n_0 (with the initial ion number n_0 and the number of non-photodetached ions n) can be described as

$$\frac{n}{n_0} = e^{-\sigma\phi t} \tag{2.2}$$

[16] with σ being the photodetachment cross section, ϕ the photon flux (photons per area unit and per time unit) and t the ion-laser interaction time. So the suppression can be increased by increasing the photon flux and/or the interaction time. The photodetachment cross section is naturally fixed. Available laser power limits the photon flux. A more promising approach is to increase the ion-laser interaction time.

Liu et al. pioneered collisional cooling of negative ion beams in a radio frequency quadrupole (RFQ) ion guide [17, 18]. It was used at the Holifield Radioactive Ion Beam Facility (HRIBF) at the Oak Ridge National Laboratory for emittance improvement and photodetachment purification of radioactive ion beams. In such an ion guide the negative ions are radially trapped by a quadrupole field and accumulate near the RFQ central axis by collisional cooling in a helium gas (also referred to as buffer gas cooling). By overlapping the ion beam with a laser beam inside the RFQ, the laser-ion interaction time can be extended to the order of ms by the buffer gas cooling process. This enables a significant improvement of attainable anion suppression. Liu et al. managed to suppress 95% of a Co^- beam by laser photodetachment in a proof of principle experiment [16]. Later they could show 99.9% suppression of S^- and O^- beams as well and improve the value for Co^- to more than 99.99% [19]. It is this very approach that is also underlying the ILIAS project.

2.2. Ion motion in a RF quadrupole ion guide

Since detailed treatments of the relevant equations can be easily found in the literature (for example [20]), a comprehensive discussion will be omitted here. The mathematical description of the ion behavior in a RFQ field will be only sketched and just the most relevant results presented.

The concept underlying the ILIAS RFQ ion cooler is that of a so-called linear Paul trap, where ions are trapped radially over the whole longitudinal extent of the trap's electrode structure by a restoring force proportional to the radial distance from the center. An electrode geometry like in figure 2.2 can approximately generate a potential of the form

$$\Phi(\vec{r},t) = \frac{\Phi_0(t)}{r_0}(x^2 - y^2) \tag{2.3}$$

in the region enclosed by the cylindrical electrodes, with the radius of the circle enclosed by the electrodes r_0, the Cartesian coordinates transversal to the beam direction x and y (with the origin on the central longitudinal axis), and a time dependent potential $\Phi_0(t)$ that is typically chosen to have the following form:

$$\Phi_0(t) = U_{\mathrm{dc}} + U_{\mathrm{rf}} \cos \omega_{\mathrm{rf}} t \tag{2.4}$$

Here U_{dc} denotes a DC voltage and U_{rf} the amplitude of an RF voltage with circular frequency ω_{rf}. In order for the derived force to be restoring in both the x- and y-direction, the time dependent potential has to be applied to the electrodes such that adjacent electrodes are oppositely charged.

The original geometry first described by Paul [21] consisted of hyperbolic electrodes. To

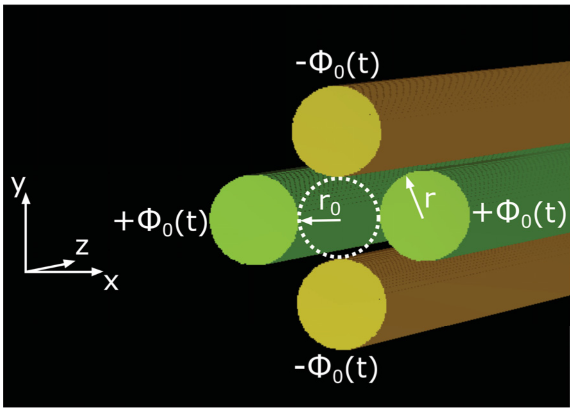

Figure 2.2.: Principle RFQ structure with cylindrical electrodes, where the green and orange electrodes are oppositely charged with respect to each other. The beam direction would correspond to the z-direction.

facilitate easy production of such a device, it is possible to replace the hyperbolically shaped electrodes by cylindrical electrodes [22]. However, for a good approximation of an ideal quadrupole field, the condition $r = 1.147\ r_0$ with r being the cylindrical electrode radius and r_0 the radius of the circle inscribed by the four electrodes (see figure 2.2) should be pursued [22, 23].
From the potential the ion equations of motion can be derived. Of course they do not account for fringe fields or longitudinal guiding fields that might be added to the trap. These equations happen to coincide with differential equations called Mathieu equations which are well known to mathematics. Their set of solutions can basically be characterized by two parameters q and a defined as

$$q := \frac{4QU_{\mathrm{rf}}}{mr_0^2\omega_{\mathrm{rf}}^2} \qquad a := \frac{8QU_{\mathrm{dc}}}{mr_0^2\omega_{\mathrm{rf}}^2} \tag{2.5}$$

with the ion mass m, ion charge Q, DC voltage U_{dc}, RF voltage amplitude U_{rf}, circular radio frequency ω_{rf} and radius of the circle inscribed by the RF electrodes r_0. Not all the solutions describe stable ion trajectories. Stability diagrams serve to illustrate how a and q have to be chosen such that the ion trajectory is stable both in the x- and the y-direction.
Figure 2.3 shows the region of stability relevant for the ILIAS RFQ ion cooler. RFQs are frequently used as mass filters for which the operating line in the stability diagram is chosen such that the ion motion is stable for only a narrow range of a and q values and therefore only for a small range of ion masses. The property to seperate masses is not relevant for the ILIAS ion cooler, which is why the time dependent potential does not have any DC component ($U_{\mathrm{dc}} = 0$ and therefore $a = 0$). The ILIAS cooler is usually operated with q around 0.5, depending on the ion species. A higher q would result in higher ion oscillation amplitudes and thereby an increased probability that ions leave the trapping

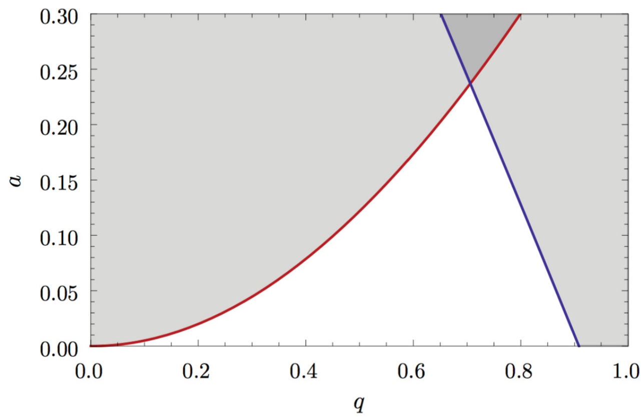

Figure 2.3.: Region of stability relevant for the ILIAS RFQ ion cooler. Taken from [9]. Light gray surfaces indicate regions that are unstable in either the x- or the y-direction, the dark gray region is unstable in both directions.

potential, as discussed below.
The exact equations of motion are rather complicated and can be expressed as fourier series. However, for $q < 0.6$ the ion motion can be approximated by a motion in a pseudopotential well

$$\Phi_{\mathrm{pp}}(r) = \frac{qU_{\mathrm{rf}}}{4}\frac{r^2}{r_0^2} \tag{2.6}$$

[24]. Thereby the ions perform an oscillation in the pseudopotential with frequency

$$\omega_{\mathrm{macro}} = \frac{q\omega_{\mathrm{rf}}}{\sqrt{8}} \tag{2.7}$$

(macro motion), superimposed by an oscillation with the frequency of the RF field ω_{rf} (micro motion). This so called adiabatic approximation can be helpful for qualitative considerations, concerning for example the maximum number of ions that can be trapped. Many losses can be expected, once the potential generated by the accumulated ions (space charge potential) exceeds the depth of the pseudopotential well. So especially when dealing with high intensity ion beams, it is favorable to increase the depth of the pseudopotential well as far as possible. This can in principle be achieved by increasing q and/or U_{rf}. However, besides being limited to the region of stability, q is linked to the ion oscillation amplitudes, which means that increasing q would lead to additional losses.

2.3. Buffer gas cooling of negative ions

By filling the RFQ volume with a light gas like helium, the radially trapped ions can be thermalized by (foremost) elastic collisions with the gas atoms. That means that their macro oscillation is damped and the mean radial and longitudinal kinetic energy trends

to an equilibrium imposed by the temperature of the surrounding buffer gas. This process confines the ion beam to a narrow region around the central axis of the cooler (minimum of the potential well) and, most importantly for isobar suppression by laser photodetachment, significantly increases the ion residence time inside the cooler. The confinement to the axis results in an improvement in overall beam emittance leading to a better beam transmissions through the cooling system than without buffer gas cooling. The achievable residence times depend on the buffer gas pressure. Higher pressure corresponds to longer residence times. The reason for this is that the number of available collision targets for the ions is larger and therefore the ions reach their equilibrium kinetic energy less far into the cooler. This will be discussed in section 5.2 where measurements on the ion residence time will be presented.
To give an idea, examples for typical parameter values for the ILIAS ion cooler obtained by simulations are an equilibrium kinetic energy of 0.08 eV, confinement of the ions within a displacement of 0.5 mm from the central axis and total ion residence times in the order of ms [9].

An important difference to well-established positive ion coolers is that negative ions are weakly bound systems, electron affinities are typically one order of magnitude smaller than corresponding ionization energies. Therefore, special care has to be taken to prevent collisional detachment when injecting negative ions into the buffer gas filled volume. In an elastic collision of an ion with energy E_{lab} in the laboratory frame of reference and mass m_i, with a neutral gas atom with m_n and negligible kinetic energy, the collision energy in the center of mass frame of reference is given by

$$E_{\mathrm{cm}} = \frac{m_{\mathrm{n}}}{m_{\mathrm{i}} + m_{\mathrm{n}}} E_{\mathrm{lab}} \tag{2.8}$$

[17]. E_{cm} ideally should not exceed the electron affinity of the ion of interest. For that reason it is essential to decelerate the ions previously to exposing them to buffer gas cooling in the RFQ (as also discussed in section 3.2).

3. The Ion Laser InterAction Setup (ILIAS)

The Ion Laser InterAction Setup (ILIAS) was built to carry out independent studies and development work on isobar suppression by laser photodetachment in an RFQ ion cooler, prior to the implementation of this technique at the injection stage of VERA. In autumn 2014 a first beam of cooled ions could be extracted from the cooler. Since then modifications have been made to improve its performance. This chapter describes the state of the setup at the end of this master's thesis project. Since work to transfer the system to the accelerator hall is already underway, this can be regarded as the final state of the test setup.

3.1. General outline

ILIAS is basically a negative ion mass spectrometer followed by an RFQ ion cooler and additional means allowing for ion-laser overlap.

The negative ions are generated in a standard single cathode cesium sputter ion source (SNICS II from National Electrostatics Corporation, Middleton, Wisconsin, USA) with a cathode voltage of 6 kV. The source is followed by an electrostatic acceleration section (up to 24 kV). Together with the cathode voltage this results in a maximum acceleration voltage of 30 kV and therefore a maximum (singly charged) ion energy of 30 keV. However, an ion energy of 23 keV was chosen most of the time because of limitations imposed by one of the 90° electrostatic benders.

An einzel lens is mounted after the acceleration section and a second one before the analyzing magnet. This section of the setup also includes adjustable horizontal and vertical slits, as well as a horizontal and a vertical electrostatic steerer.

A double focusing 90° analyzing magnet allows for mass selection in a range up to 560 u for singly charged 30 keV ions. The magnet is followed by a vertical magnetic steerer and another set of vertical and horizontal slits.

For the experiments targeted to measure the ion residence time for ion currents of various intensities injected into the cooler, insertable attenuation foils were used that are mounted in the beam line cross after the magnetic vertical steerer, as well as near Faraday cup FC2 after the cooler section.

The beam line section accommodating the ion cooler including the RF setup and other directly linked electronics equipment is located on the same high voltage platform (up to

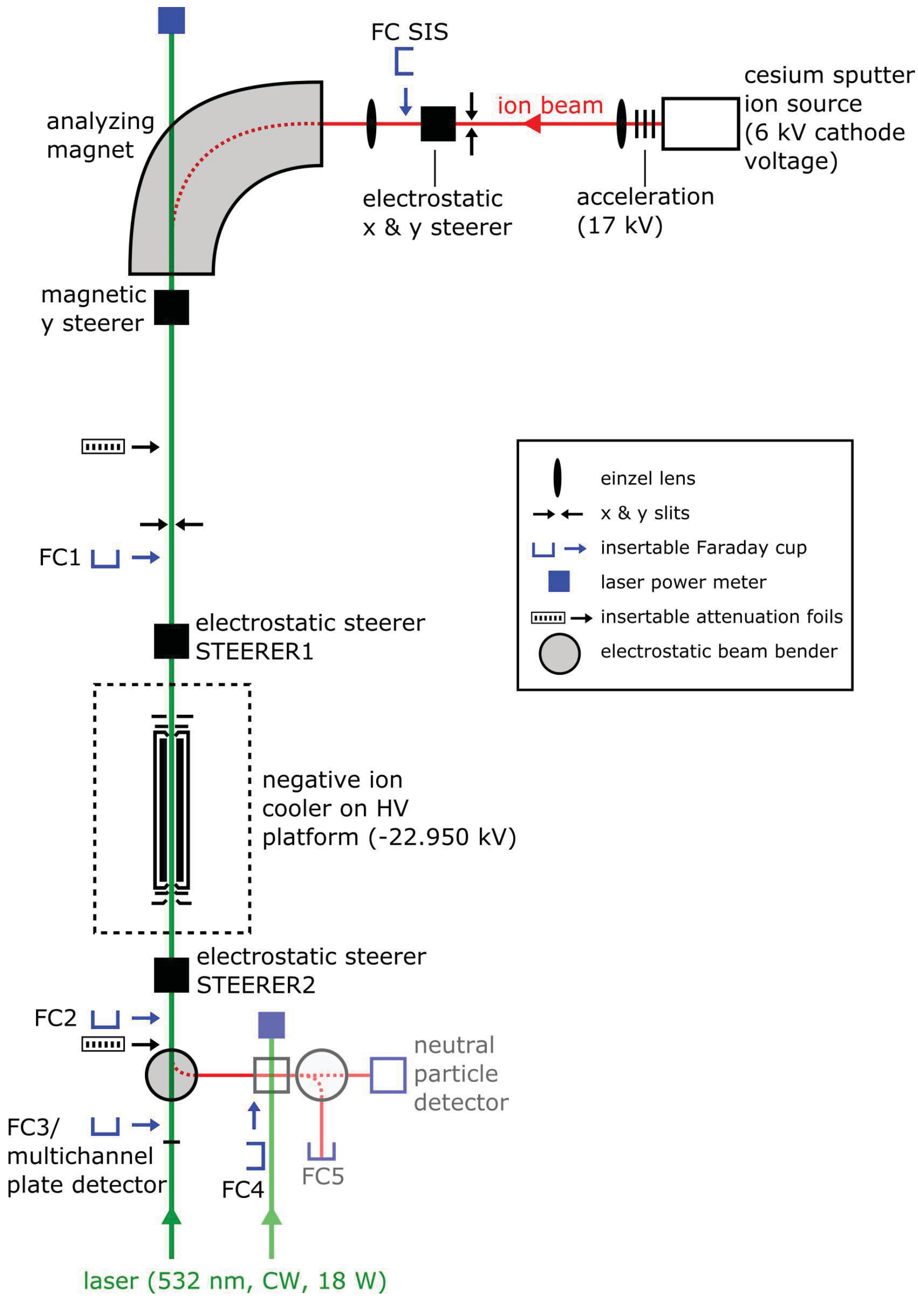

Figure 3.1.: Scheme of the Ion Laser InterAction Setup (ILIAS). The faint region following Faraday cup FC4 indicates a part of the setup for orthogonal laser ion overlap which is not relevant for the experiments described in this thesis.
Typical settings for the acceleration voltages are given. The nominal kinetic energy of ions entering the cooler (injection energy) is determined by the difference between the initial acceleration voltage and the cooler high voltage. In the above case it would amount to 50 eV.

-30 kV), electrically insulated from the rest of the setup by ceramic insulators.

The installation of two compact steerers both right in front and right after the ion cooler section was part of this master's thesis project. Their construction and their impact on

the transmission through the ion cooler will be a subject of section 4.1 and section 5.1.
The ion beam extracted from the cooler is deflected by 90° by a quadrupole deflector (electrostatic bender) from the axis of collinear ion laser overlap. Naturally the laser beam would not be able to pass Faraday cups FC1 and FC2 if they were inserted. So during laser photodetachment experiments, the ion current has to be measured in either FC4 or FC5.
Actually only the part up to Faraday cup FC4 is relevant for this thesis (non-faint region in figure 3.1). ILIAS is in principle also suited for orthogonal laser ion beam overlap (crossed beams configuration) which is why an alignment apparatus, another 90° bender with a Faraday cup in the sidearm and a neutral particle detector to detect neutral detachment remnants follow FC4. Information about crossed beams experiments conducted with ILIAS can be found in [9, 10, 25].
For all experiments involving laser-ion overlap described in this thesis, the laser setup consisted of a single frequency CW solid-state laser (VERDI-V18 from Coherent, Santa Clara, California, USA) with 532 nm wavelength and 18 W maximum power. For collinear overlap inside the ion cooler the laser beam can enter through a window after FC3. It exits behind the analyzing magnet where the transmitted laser power of typically 10 W to 12 W, depending on the tuning, is measured with a power meter.
Reliable detection of currents down to 1 pA is realized by insertable Faraday cups on several positions of the setup (FCSIS, FC1, FC2, FC3, FC4 and FC5). For the residence time measurements FC3 was replaced by a microchannel plate detector. Together with current measurement possible on the entrance and the exit aperture of the ion cooler (see the following section) and the slits, these are the only ion beam diagnostic tools available. It is not possible to further analyze the beam for example with respect to ion species composition.
Most components of the setup can be controlled via a commercial automation system (Beckhoff Automation, Verl, Germany).

3.2. The RF quadrupole ion cooler

3.2.1. Injection and extraction

The cooler section ranging from the deceleration to the acceleration electrodes (drawn red in figure 3.2) is on a high voltage platform, including all the electronics for the components of this section. The cooler potential can be as high as -30 kV with respect to the ground potential of the rest of the setup. As mentioned in the principles section, it is crucial to decelerate the negative ions prior to the injection into the cooler to prevent collisional detachment. Taking as an example a $^{63}Cu^-$ ion and a helium gas atom, equation 2.8 tells us that a center of mass collision energy equal to the electron affinity of copper (1.24 eV [26]) corresponds to a lab energy of the ion of 20.8 eV. So ideally the ion injection energy should

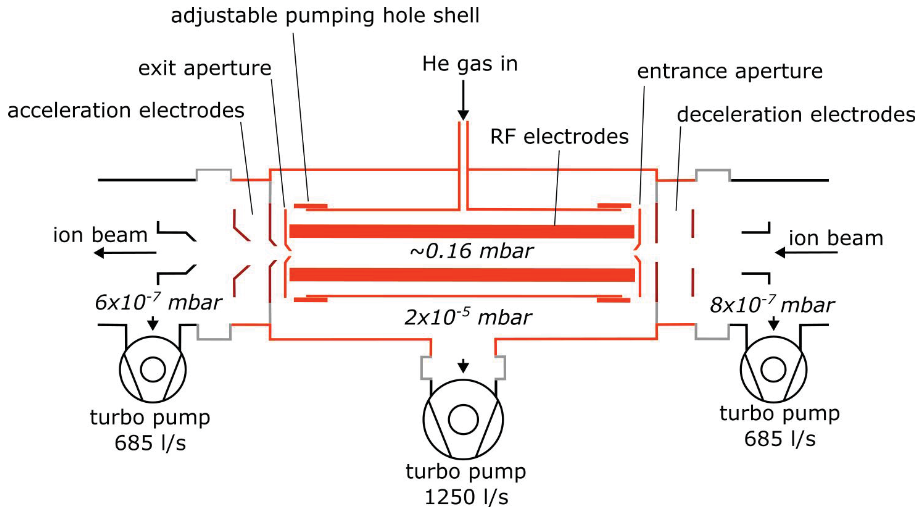

Figure 3.2.: Schematics of the ILIAS ion cooler. Not to scale. The red section is on cooler high voltage, insulated from the rest of the beamline by ceramic insulators indicated in light gray.

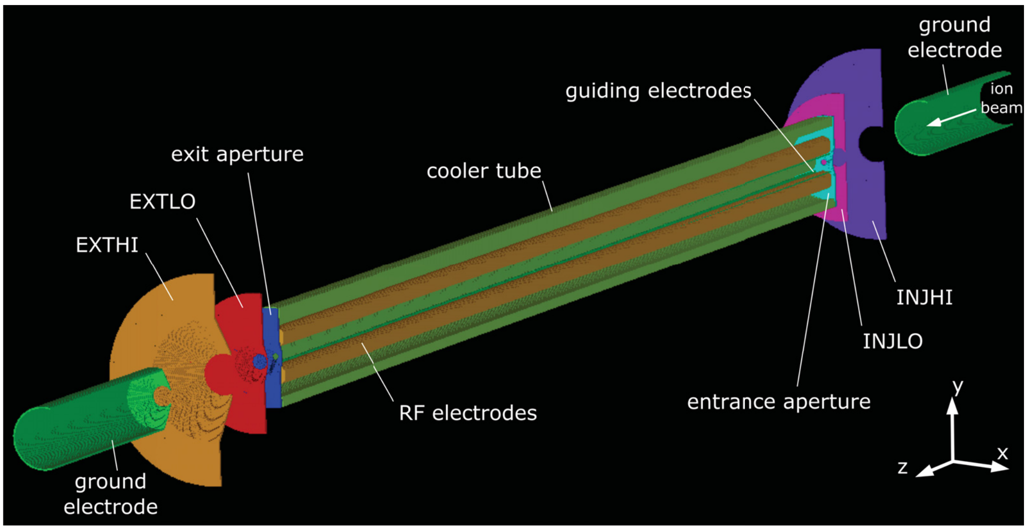

Figure 3.3.: Longitudinal section through the cooler electrode structure. Illustration of the simulation geometry described in section 4.2. Details like for example the pumping holes with the corresponding shells, the electrode holders and the gas inlet are not considered. The ground electrodes are not on cooler high voltage but on beamline ground.

be below that value to avoid collisional losses. In reality an optimum in the transmitted ion current can be found for an injection energy of about 50 eV [9]. The reason is that ion losses are not just caused by collisional detachment but also by increased beam divergence resulting from ion deceleration. The optimum somewhat presents a compromise between the two. From an ion optics viewpoint, the setup is not fully optimized due to spatial limitations. Improvements can be expected once the setup will be coupled to VERA.

In figure 3.3 the cooler structure including the deceleration and acceleration electrodes and the RFQ section is shown. The acceleration section basically mirrors the deceleration section, except for the conical shape of the acceleration electrodes. INJLO and EXTLO each can be supplied with up to 1.25 kV, and INJHI and EXTHI with up to 12.5 kV positive DC voltage with respect to the cooler potential of up to -30 kV. The ground electrodes are just passive components on beamline potential. The ion optics is further discussed in section 4.2 and in [9].
The ion beam enters the tube containing the RFQ structure through a partially conically shaped aperture with an opening diameter of 3 mm. On the extraction side an identically shaped aperture covers the tube. Both apertures are insulated from the tube and can be used to measure the current induced by ions terminating on them. To that end they are connected to low noise current preamplifiers (SR570 from Stanford Research Systems, Sunnyvale, California, USA).

3.2.2. RFQ structure

The cylindrical RF electrodes have a radius r of 5 mm and are 95 cm long. The radius of the circle inscribed by the RF electrodes r_0 is nominally 4.37 mm. So $r/r_0 = 1.144$, being close to the optimal quadrupole field approximation ratio for cylindrically shaped electrodes of 1.147 given in section 2.2.

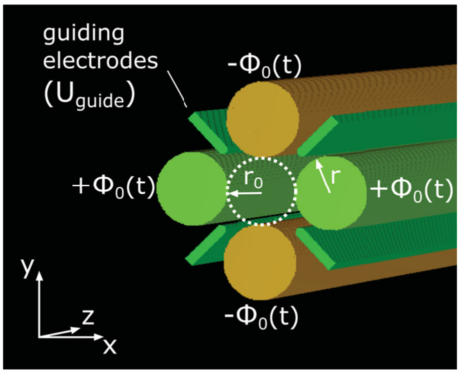

Figure 3.4.: RFQ electrode structure. Here $\Phi_0(t) = U_{\mathrm{rf}} \cos 2\pi f_{\mathrm{rf}} t$. Typical operation values would be $U_{\mathrm{rf}} = 200$ V, $f_{\mathrm{rf}} = 2$ MHz and $U_{\mathrm{guide}} = -30$ V.

To generate the RF voltage a small amplitude sine voltage from a frequency generator is amplified by an RF power amplifier and split in two components phase shifted with respect to each other by 180° using a simple transformer configuration (balun = balanced to unbalanced converter). These voltage components are supplied to the cylindrical electrodes such that the voltages on adjacent electrodes are phase shifted. The RF setup used is non-resonant and very limited in the attainable amplitudes at frequencies above 2 MHz. This makes it especially difficult to work with light ions like for example carbon, where the lighter mass has to be compensated by a higher frequency to get to the optimal value of

the parameter q (formula 2.5). Improvements in this respect can be expected with a new resonant RF setup that has been designed and is waiting for its use. First tests showed amplitudes up to 400 V over the complete required frequency range.
Maximum transmissions are found for $q = 0.45$ for $^{36}Cl^-$, $q = 0.50$ for $^{27}Al^{16}O^-$ and $q = 0.55$ for $^{63}Cu^-$ [9].
In between the RF rods, electrode bands (figure 3.4) generate a small potential gradient to guide the thermalized ions toward the cooler exit. From hereon they shall be referred to as guiding electrodes. The longitudinal field gradient results from slightly tilting these electrodes, meaning that the distance through the center between opposing guiding electrodes is greater by 1.2 mm at the end of the RFQ corresponding to an opening angle of each electrode of 0.036°. A negative voltage of up to -650 V with respect to the cooler platform potential can be applied. For injected ion currents of several 100 nA, the influence of the guiding electrode potential is almost negligible, only a small maxmimum in transmission can be found for a voltage of -30 V applied to them. Their influence on the ion residence time for various injected currents will be a subject of section 5.2.

3.2.3. Buffer gas and vacuum

In full operation, the cooler tube is typically filled with 0.1 mbar to 0.2 mbar helium gas through a gas inlet in the center. In the ILIAS laboratory also argon and nitrogen are in principle available and can be used as buffer gases. However helium is by far the most appropriate choice, as is shortly addressed in section 5.3. The gas pressure is measured in the wide inlet, so it presumably reflects the pressure in the center of the cooler tube. However the pressure profile throughout the cooler tube is unknown. Measurements presented in section 5.3 suggest that the pressure near the tube ends is significantly lower than in the central section.
It is crucial to prevent the buffer gas in the cooler tube from leaking into the rest of the beamline and destroying the vacuum. A strong turbomolecular pump keeps the vacuum in that region at about 10^{-5} mbar (see figure 3.2). The EXTLO and INJLO electrode lenses serve as pumping barriers, such that gas can enter the rest of the beamline only through their 10 mm diameter openings. Just outside these regions on both sides another two turbo pumps are located near the ground electrodes.

4. Development and simulations

This chapter deals primarily with the construction of two novel compact beam deflectors that were crucial for the improvement of the transmission through the ion cooler. The second part describes SIMION 8.1 [28] simulation studies on the cooler injection and extraction ion optics which are important for the connection of the system to VERA.

4.1. Construction of a compact two dimensional beam deflector

When a beam of cooled ions was extracted from the cooler for the first time, the transmission from Faraday cup FC2 to the cups FC4 or FC5 was very poor. Only up to about 25% of the current measured in FC2 could be expected in FC4, even less in FC5. These losses were suspected to be either due to bad ion optical properties of the electrostatic bender or an angular offset of the beam beeing extracted from the cooler caused by a misalignment of the extraction section. Because of the statistical process of collisional cooling, the information on the injection trajectories has faded away for the beam exiting the cooler. Hence the extraction section of the ion cooler is the starting point for the rest of the beamline similar to the ion source for the injection section. During these first experiments there wasn't any component compensating for the mentioned misalignment. For that reason it was decided to install a beam deflector (STEERER2) into a beamline cross piece following the ion cooler (see figure 3.1).
Some time later another steerer, STEERER1, of the same type was built and installed in a crosspiece right in front of the ion cooler section. Its purpose was to correct for steering effects from the injection lenses or other components in front of the cooler, such that a coaxial injection could be achieved.
The need for additional steerers for ILIAS was taken as an opportunity to construct a prototype for a novel kind of steerer that could later be replicated for use at VERA. Limited space for additional components at VERA calls for a device with minimum space requirements, that can be easily manufactured in the VERA mechanics and electronics workshop at low cost. It should simultaneously allow for both horizontal and vertical beam deflection.
This subchapter describes the construction of STEERER1 (see figure 3.1), the mechanical design as well as the associated electronics setup. The concept was initially developed by Peter Steier, the construction and installation was the responsibility of the author.

4.1.1. Principle

The objective of the steerer is to generate a homogeneous field in any desired direction transversal to the ion beam direction, while occupying only very little precious space in the beamline. This is accomplished by eight rectangular electrode plates mounted in an octagonal structure (figure 4.1). Four electrodes can be supplied with positive voltages from 0 V to 1.25 kV with respect to the beamline ground. Every electrode is electrically connected to each of its neighbouring electrodes via a 100 MΩ resistor. As a result each of the passive electrodes takes the average potential of its adjacent voltage supplied electrodes.

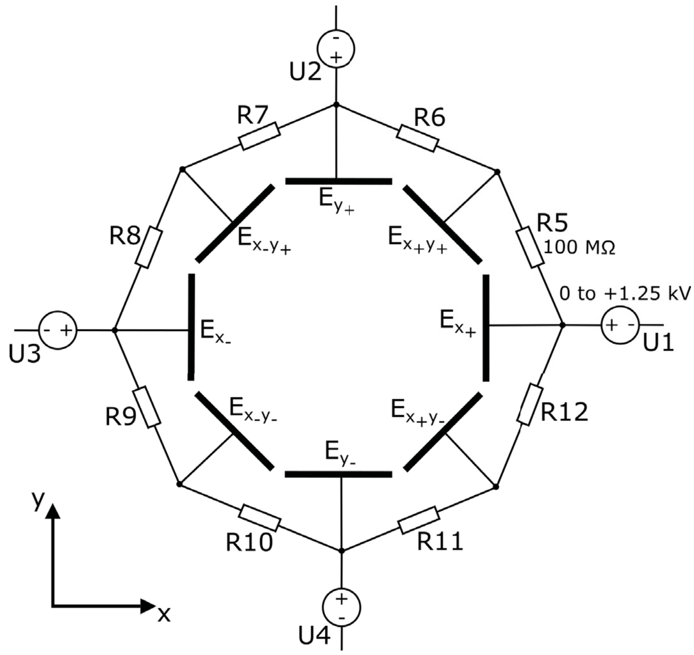

Figure 4.1.: Cross section view of the principle electrode structure and the main electronic components. The ion direction of flight (z) would point into the schematic drawing. All the component designations follow those used in the circuit diagrams figure 4.5 and figure 4.6.

In the end the steering should be controlled by two parameters, one for the desired deflection in the x-direction (horizontal) and one for the y-direction (vertical), respectively. Those parameters control the voltage setting on each of the four HV power supply modules. The resulting deflection field is a superposition of the horizontal with the vertical electrostatic field, generated by the potential difference $U_{y-} - U_{y+}$ between the electrodes E_{y-} and E_{y+} and the potential difference $U_{x-} - U_{x+}$ between the electrodes E_{x-} and E_{x+} respectively. See figure 4.1 for the electrode designations. In case of a homogeneous field leading to a deflection in the vertical direction only, it is apparent that U_{x-} and U_{x+} would both have to be set to the average value of the potential difference in the y-direction (vice versa for the case of a field in the horizontal direction). More generally stated, a mandatory condition would be that the x- and y-potentials in the center of the steerer have to be equal. Let's denote the overall control parameters by c_x and c_y which shall both range from $-U_{max}$ to $+U_{max}$, where U_{max} is the maximum voltage of each of the four power supplies. Setting c_x to $+U_{max}$ corresponds to a maximum deflection in the positive x-direction (for negatively charged particles), setting it to $-U_{max}$ corresponds to a maximum deflection in the negative x-direction. Same for c_y. To work out the relation between the control parameters and the voltage settings on the power supplies U_{x+}, U_{x-}, U_{y+} and U_{y-}, it is helpful to first define four auxiliary variables:

$$h_{x_+} = +\frac{c_x}{2} \qquad h_{x_-} = -\frac{c_x}{2}$$

$$h_{y_+} = +\frac{c_y}{2} \qquad h_{y_-} = -\frac{c_y}{2}$$

Setting them to the above values guarantees that the potentials in the center are equal for the x- and the y-field (both are 0). To get the real voltage settings for the four main electrodes from those auxiliary variables

$$k = |min(h_{x_+}, h_{x_-}, h_{y_+}, h_{y_-})|$$

has to be added to each of them to shift the settings to positive numbers, since only positive voltages can be generated by the high voltage power supplies. Therefore one obtains for the voltages applied to the field electrodes:

$$U_{x_+} = h_{x_+} + k \qquad U_{x_-} = h_{x_-} + k$$

$$U_{y_+} = h_{y_+} + k \qquad U_{y_-} = h_{y_-} + k$$

In figure 4.2 results from a SIMION 8.1 simulation are shown. The corresponding SIMION geometry file can be found in appendix A.1. For three different control parameter settings equipotential contour plots for a transversal section through the front part of the steerer are shown. The control parameter settings of (b), (c) and (d) correspond to a deflection of negatively charged ions north, north-northeast and northeast respectively. The field in the center seems fairly homogeneous for each of the three settings.

4.1.2. Mechanical design

The design focus was on fast and easy production and minimum space requirements. Apart from protruding screws the steerer without holders takes a cubic volume of about 10 cm × 10 cm × 10 cm. It was designed such that it would fit into an opening of a DIN 160CF 6-way cross piece. To that end, the steerer was mounted on a DIN 160CF flange. The control circuit is located in a box on the outside, electrical connection to the electrodes is established via a vacuum current feed-through.

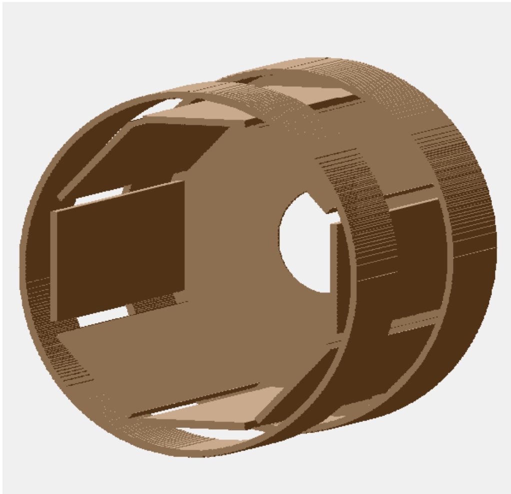

(a)

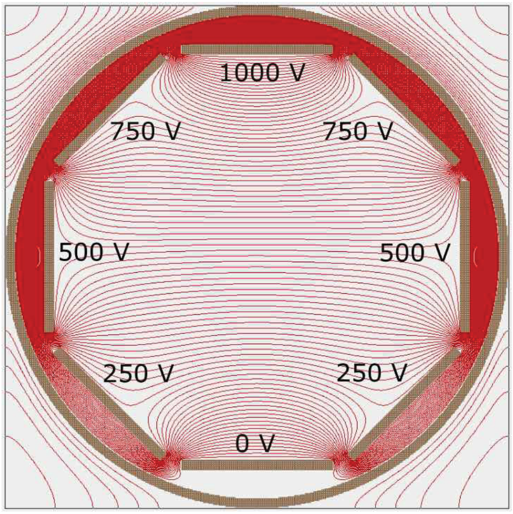

(b) $c_x = 0$ and $c_y = 1000$

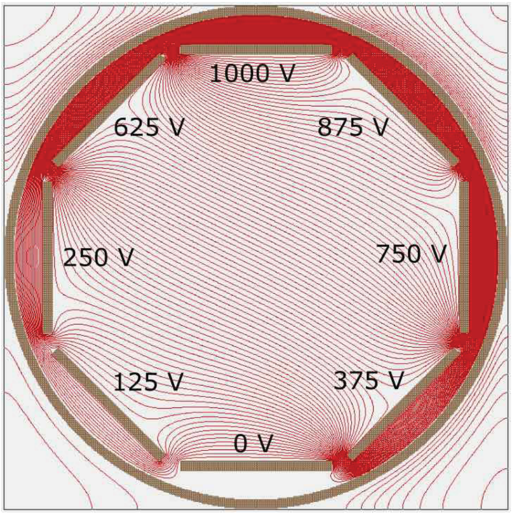

(c) $c_x = 500$ and $c_y = 1000$

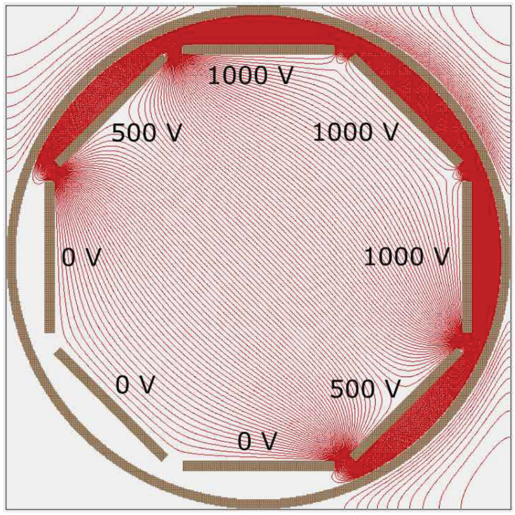

(d) $c_x = 1000$ and $c_y = 1000$

Figure 4.2.: (a) SIMION 8.1 simulation geometry. See appendix A for the geometry file of geometry (a). (b), (c) and (d) show equipotential contour lines on a transverse section through the geometry for three different deflection field settings.

The deflector consists of 8 aluminium electrode plates, mounted on the inside of two steel rings with an inner diameter of 10 cm in an octagonal arrangement (see figure 4.3). The front side is covered by an aperture with a 30 mm opening. The bolts and nuts fixing the electrodes are insulated from the steel rings by ceramic spacers. L-shaped holders are welded onto the rings. The structure is suspended on a DIN 160 CF to DIN 40CF reducing flange via two threaded rods to allow for vertical adjustment. They are fixed on the L-shaped holders by nuts, where the holes on the holders are elongated in the x-direction to also allow for slight horizontal adjustment of the structure.
Electric connection is established via a DIN40CF 10-fold current feed-through. Each one

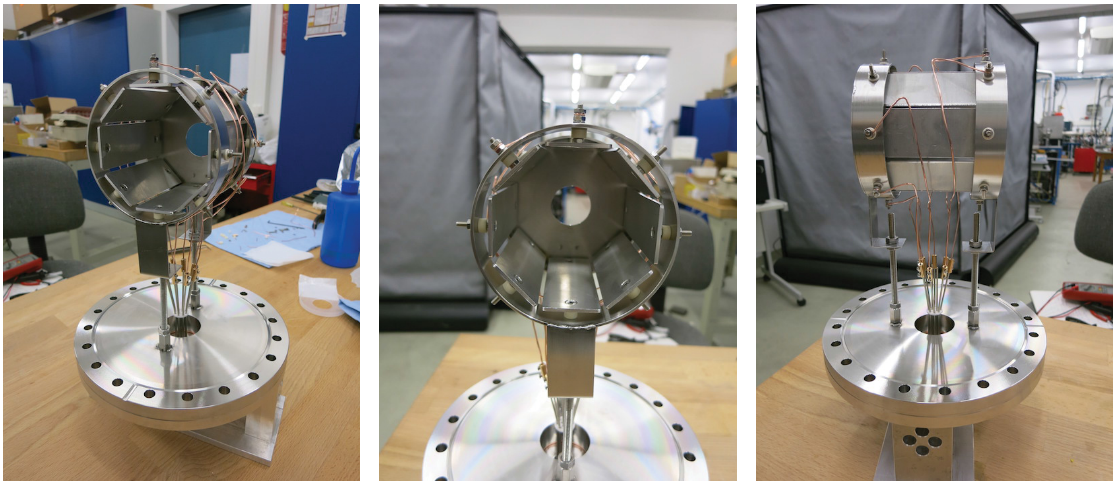

Figure 4.3.: Photographs of STEERER1. The ion beam is to enter the steerer through the side covered by the aperture. The steerer is shown upside down, it is introduced into the beamline through the top opening of the cross piece.

of the 8 steerer electrodes is connected to one of the feed-through pins by copper wire clamped between two nuts on the outer ends of the screws fixing the electrodes. UHV-in-line connectors of BeCu establish the connection between each wire with one of the pins of the current feed-through.
The individual mechanical parts needed are quite simple, construction plans are therefore omitted, but a more detailed verbal description is given for eventual future replication of the device:

Part specifications:

- Eight electrode plates 92 mm long and 31.5 mm wide from 2 mm thick aluminium sheet. On each end of each electrode a hole for a countersunk M3 screw is located 8 mm from the edge.

- Two standard stainless steel beam pipe segments serving as electrode holders. Inner diameter 100 mm, 20 mm wide. The front holder is covered by an aperture (1 mm thick steel sheet) with an opening diameter of 30 mm. L-shaped holders are welded onto them (see figure 4.3 right) with holes for the threaded rods elongated in the x-direction.

- Sixteen M3 countersunk screws, forty M3 nuts, sixteen splitted washers and sixteen sets of ceramic split bushes (BGB-M3 from tectra, Frankfurt am Main, Germany) to fix the electrode plates on the rings.

- One CF reducing flange DIN 160CF to DIN 40CF (ZL 160040-304 from VACOM, Großlöbichau, Germany). Long M6 nuts are welded onto them to accomodate the threaded rods holding the steerer. The nuts are slitted on the flange side to prevent air from being trapped in them, that could contaminate the vacuum.

- One DIN 40CF 10-fold current feed-through (CF40-HV2-10-CE-AM16, VACOM). Only 8 pins in use.
- Copper wire and 8 barrel type connectors (EK-LK-CB16, VACOM) to connect each electrode with a pin from the feedthrough.
- Two M6 threaded rods, 10 cm long and six M6 nuts to fix the steerer structure on the flange.

4.1.3. Electronics

The steerer control circuit was assembled on a perfboard and is contained in a metal box sitting on top of the flange accommodating the steerer (figure 4.4).

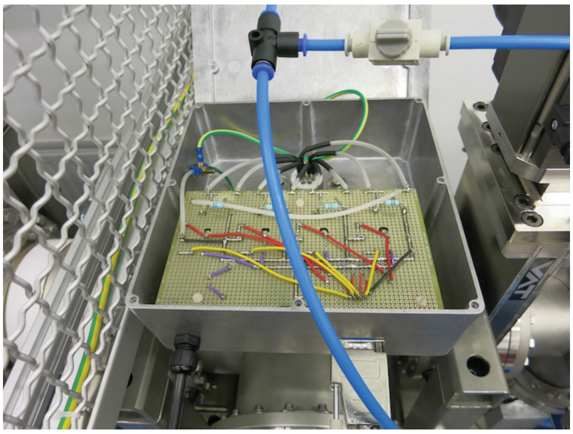

Figure 4.4.: Box containing the circuit on top of the steerer flange. The line voltage cable feeding the power adaptor for the HV power supplies and the 9 pole D-sub connector for the connection to the ILIAS control system are located on the front side. In the back section of the box the plug connections to the vacuum feed-through pins are visible.

Figure 4.6 shows the full circuit diagram. The circuit design was partly adopted from a different steerer previously built for VERA [27]. Figure 4.5 includes pictures of the circuit board together with an eye-guiding orientation diagram.
9 connections link the circuit to the ILIAS control system. They include one read and one control voltage (each 0 V to 5 V) for each of the four electrode HV power supplies, as well as a common ground identical to the beamline ground. The method to get from two overall control parameters to the voltage settings for the four HV power supplies described above is implemented in a short program in the automation system controlling ILIAS. A standard 230 V and 50 Hz AC line voltage powers the 15 V DC circuit power supply. 8 plug connections connect the circuit board with the vacuum feed-through pins of the electrodes, where the head of the feed-through is also enclosed by the metal box. As

mentioned in the principle section, the electrodes are circularly linked to each other via 100 MΩ resistors to apply voltages to the passive electrodes. At first it was intended to use 24 MΩ resistors, however during first tests it turned out that this resulted in too much current flowing back to the HV power supply modules, causing unintended behavior.

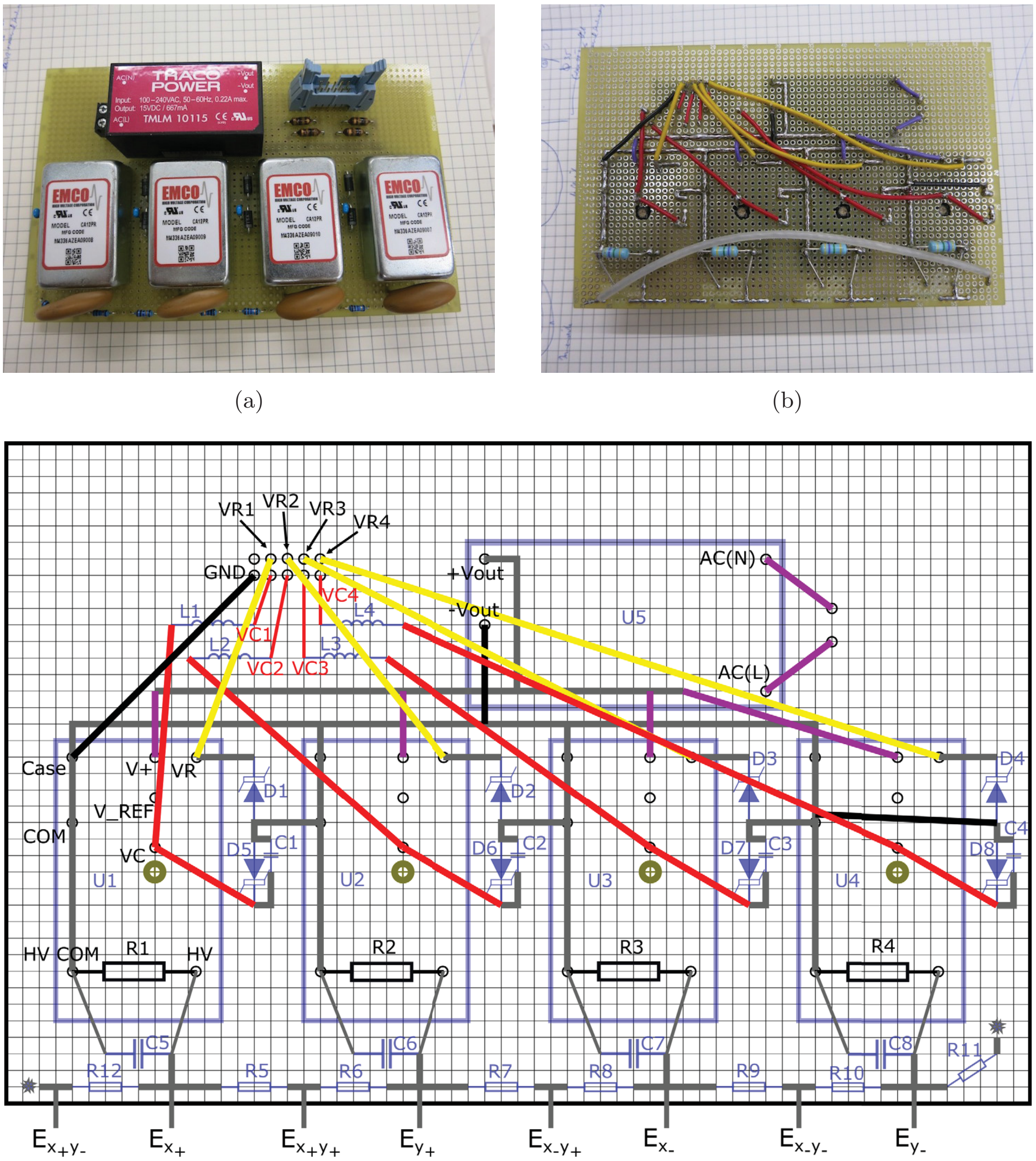

(c)

Figure 4.5.: Component side (a) and solder side (b) of the steerer circuit board. (c) shows an orientation plan of the solder side using the designations of the steerer circuit schematic in figure 4.6. The components on the back are represented in light blue.

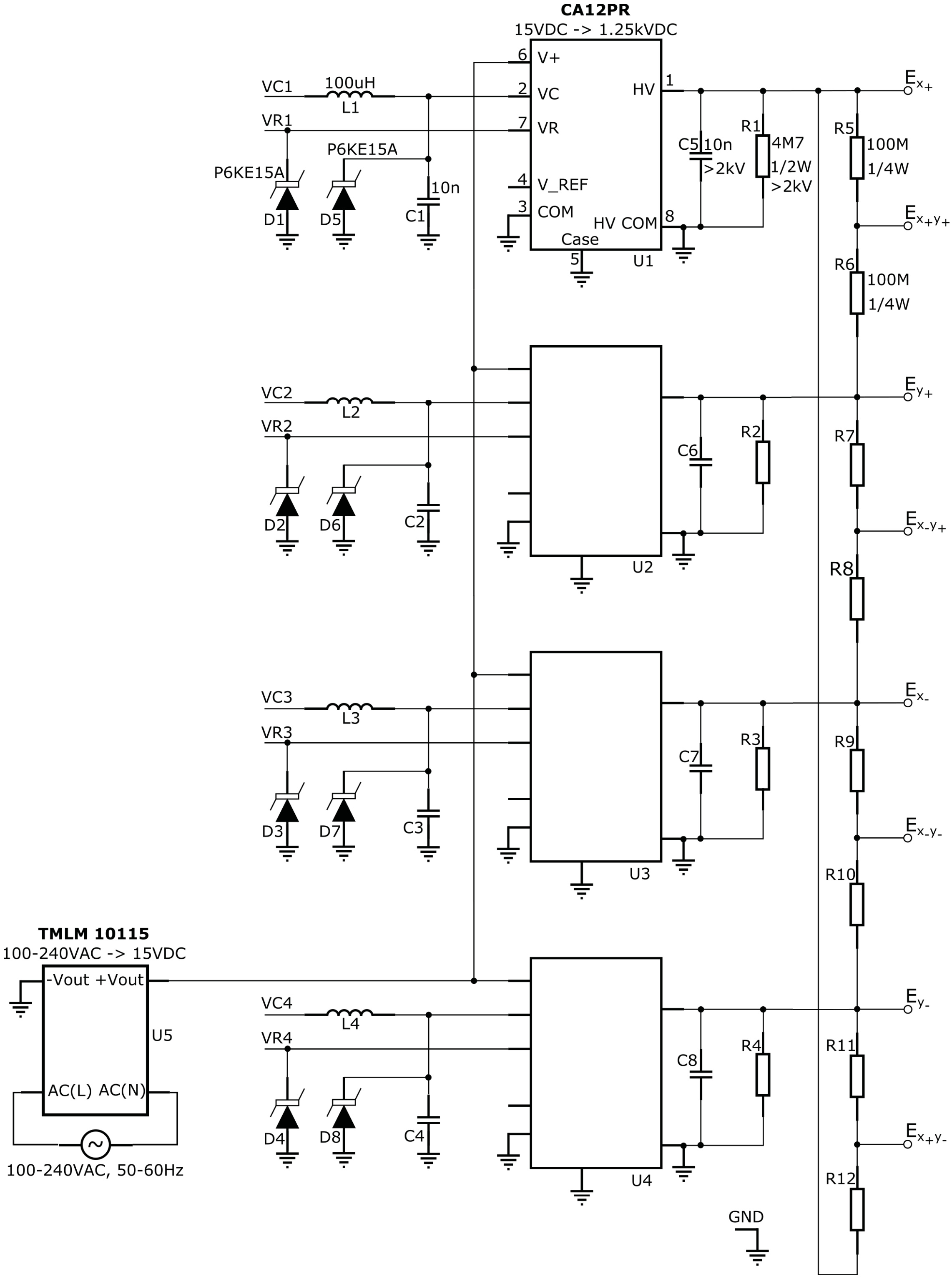

Figure 4.6.: Steerer control circuit diagram. Based on a circuit previously developed for a steerer used for VERA [27]. Only one of the four identical blocks is fully labeled.

4.2. Ion optics simulations

With the coupling of the laser photodetachment system to VERA lying ahead, questions concerning the optimal shape of the ion beam injected into the cooler were to be addressed. By changing the distance between the RFQ section and the magnet in the dedicated VERA beamline section, the position of the beam waist can be influenced to a certain degree within given spatial limitations. The same applies for the extracted beam and the electrostatic analyzer that will be following the cooler. Not least due to various optimizations, the ion optical properties of the system cooler + deceleration and acceleration lenses are not well known. In this subchapter a simulation study is presented. It focused on determining where the beam waist has to be located for the beam injected into the cooler in order to maximize the transmission.
The simulations were carried out using SIMION 8.1 [28], an ion optics simulation program. It basically can calculate electrostatic (or magnetostatic) fields and thus ion trajectories in a given electrode geometry by solving the Laplace equation using a finite difference method.

4.2.1. Simulation geometry

The electrode geometry for the following simulations was defined in a separate geometry file. With regard to potential future simulations where this file could be reused, a geometry for the entire cooler system was written. It is primarily based on preexisting SIMION 8.0 simulations of the injection and extraction section. Components for which detailed construction plans exist were redesigned accordingly. Certain dimensions were updated when direct measurements during cooler maintenance revealed discrepancies.
SIMION 8.1 allows for the use of macros in the geometry definition files (written in the language LUA), which enabled most of the following convenient features:

- The geometry is scaled so that dimensions are given in millimeters instead of grid units.
- To change the grid density, only one parameter has to be altered. The geometry will be adjusted automatically.
- The z-positions (beam direction) of each component is given relative to a reference position, which corresponds to the start of the cylindrical RF electrodes. When a component's position has to be altered, only one variable has to be changed. The file doesn't have to be entirely redefined.
- If only a certain part and not the whole length of the geometry is to be simulated, the longitudinal section can be freely chosen. To that end, two parameters define the start and end position of the simulation section with respect to the reference position.

In figure 4.7 a scheme of the geometry is shown, together with longitudinal dimensions. The complete file is given in appendix A.2.

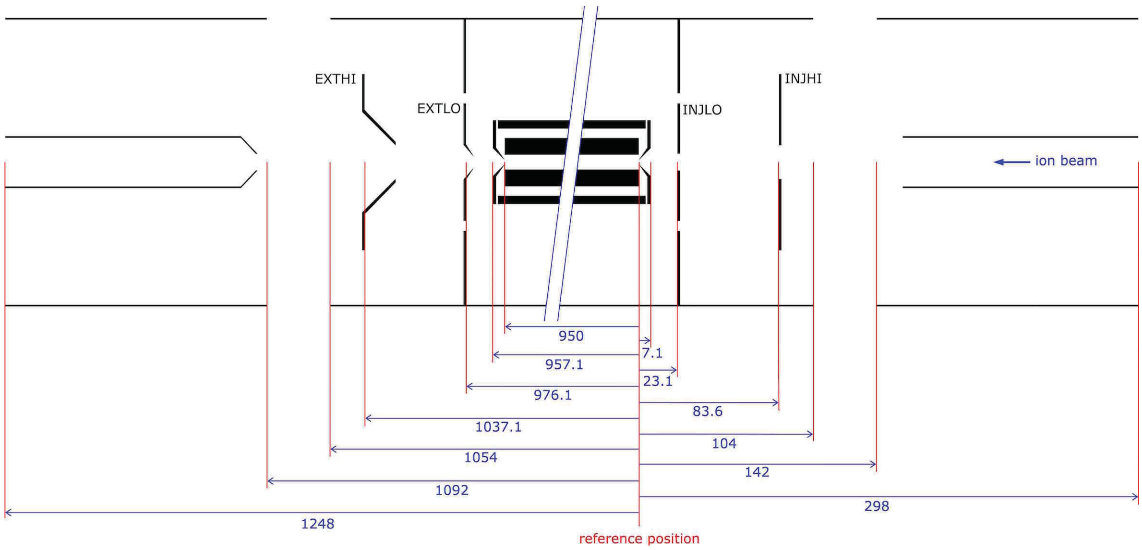

Figure 4.7.: Scheme of a longitudinal section through the 3D geometry defined by the geometry file given in appendix A.2. The middle section of the RFQ is left out for representation purpose. Some longitudinal dimensions are given in mm with respect to the reference position.

4.2.2. Injection ion optics

To be able to systematically evaluate the cooler acceptance for a given ion beam, the transmission 95 mm into the RFQ was recorded for different lens voltage settings. A user program (see appendix A.3) was written, that could automatically vary the lens voltages in between consecutive runs and for each run write the voltages and the corresponding transmission into a file.

The simulated section for the following simulations ranged from the outer extent of the complete geometry on the injection side (-298 mm from the reference position in figure 4.7), to 100 mm into the RFQ electrodes (+100 mm from the reference position). In order for the simulations to run reasonably fast, a grid density of 4 grid units/mm was chosen. This required to thicken the cone of the injection aperture, to prevent ions from passing through it (see the geometry file in appendix A.2 for details).

The comparison of differently shaped beams with respect to the suitability for the cooler injection requires that their emittance is kept constant. To define a beam with a given emittance, the *emittance.lua* program from the SIMION 8.1 examples [29] was imported into the simulation's user program. It was only slightly modified to allow for the selection of a plane transversal to the beam direction for which the r.m.s. emittance in both the x- and y-direction is calculated.

The ions (1000 particles per run) were started from a filled circular distribution that was mapped to a pupil (also with a filled circular distribution) 500 mm away, both with the center on axis. For the definition of a parallel beam, the radii of the pupil and the source distribution were equal. This radius was varied until the beam was found to have an appropriate emittance (see below). This was the case for a radius of 2.65 mm. The source position was 100 mm and the pupil 600 mm in front of the entrance aperture.
To simulate a beam waist, the pupil distribution radius was set to 1 mm, according with an assumed beam width of 2 mm at the waist, and the radius of the source distribution was set to 7 mm to approximate the chosen emittance. The source and pupil position varied during the simulations (with constant distance between them) to study the acceptance as a function of the waist position.

The emittance of an uncollimated 70 keV beam extracted from Source2 of VERA was measured to be 9.51 $\pi \cdot \mathrm{mm} \cdot \mathrm{mrad}$ [27]. This emittance however is defined differently than the emittance calculated with the user program. It is related to the simulation emittance $\varepsilon_{\mathrm{sim}}$ by $\varepsilon_{\mathrm{sim}} = \sqrt{\frac{7}{3}} \cdot \frac{1}{4} \cdot \varepsilon_{\mathrm{vera}}$. The factor $\sqrt{\frac{7}{3}}$ scales from 70 keV to 30 keV and the factor $\frac{1}{4}$ accounts for the difference of the 1 σ r.m.s. emittance from the simulation and the 2 σ r.m.s. emittance used for the VERA measurement. Taking this into account, the emittance of Source2 scaled to the context of the simulation would be 3.63 $\pi \cdot \mathrm{mm} \cdot \mathrm{mrad}$.
The ions initial parameters in the simulations (position, direction, energy) are (pseudo) randomly defined within the given distributions at the beginning of each run. An average over ten measurements of the emittance[1] of the beam with waist revealed a value of (3.48 ± 0.09) $\pi \cdot \mathrm{mm} \cdot \mathrm{mrad}$ for the x-direction and (3.50 ± 0.10) $\pi \cdot \mathrm{mm} \cdot \mathrm{mrad}$ for the y-direction. For the parallel beam an average value of (3.51 ± 0.08) $\pi \cdot \mathrm{mm} \cdot \mathrm{mrad}$ for the x-direction and (3.47 ± 0.07) $\pi \cdot \mathrm{mm} \cdot \mathrm{mrad}$ for the y-direction was found. The requirement 3.63 $\pi \cdot \mathrm{mm} \cdot \mathrm{mrad}$ was sufficiently approximated.

The 1000 ions per run were defined with mass 36 amu ($^{36}Cl^-$), charge -1 e and an initial kinetic energy of 30 keV (gaussian distribution with 10 eV FWHM). This initial energy distribution did not account for the high energy tail typically found for sputter ion sources, but at least added a realistic energy spread to the definition [30]. 30 keV will be the ion energy prior to the ion cooler in the new VERA beamline section, as opposed to the 23 keV typically used for ILIAS.
The guide electrode voltage was set to -50 V throughout all simulations, corresponding to a longitudinal field of 3.7 V/m. The RF electrode voltage with a frequency of 2.6 MHz (appropriate for $^{36}Cl^-$) and an amplitude of 200 V was simulated by the user program. To make sure that the ions started in different phases of the RF voltage, the ion time of birth was randomized.

[1] The emittance was measured in the field free region before the ions enter the deceleration section.

The cooler high voltage was set to -29.950 kV for an injection energy of 50 eV, -29.975 kV for an injection energy of 25 eV and -29.925 kV for an injection energy of 75 eV.
The INJHI and INJLO lens voltages were varied within the maximum voltages of the power supplies, 0 to 12.5 kV for INJHI and 0 to 1.25 kV for INJLO, each with respect to the cooler high voltage. Thereby INJHI was scanned in 1000 V and INJLO in 100 V steps.

The simulation also included buffer gas in the RFQ tube. To that end, the hard sphere collision model implementation *collision_hs1.lua* from the SIMION 8.1 example set [31] was imported into the user program unchanged. The collisions were only activated inside the RFQ tube, once the ions fully passed the injection aperture. A buffer gas pressure of 1 Pa (0.01 mbar) was used for all simulations. The temperature was set to 300 K, the gas atom mass to 4 amu and the cross section for the He-Cl^- collision to $3.24 \cdot 10^{19}$ m^2. These settings were adopted from [9] where more information about the hard sphere collision model in SIMION simulations can be found. All the other parameters were left at their default values.

The transmission in the simulations is defined as the ratio of the number of particles that reach more than 95 mm into the RFQ electrode structure within a radius of 4.37 mm from the axis (radius inscribed by RF electrodes) to the number of generated particles (1000).
The program can switch between basically three simulation modes. The first mode automatically performs multiple runs, one for each lens voltage setting and records the voltages and the transmission. Thereby a minimum and a maximum voltage as well as an increment voltage has to be given for each of the two lenses. A second mode allows for an emittance measurement on a given plane transversal to the beam direction. The third simulation mode allows for basic single-run simulations without the voltage variation, data recording and emittance measurement features.

The first simulation used a parallel beam with 50 eV injection energy (see figure 4.8). The data is presented once as a contour plot with 5% difference between each level, and once as a bar diagram to emphasize the discrete data steps. This simulation was repeated for different waist positions of the injected beam (see figure 4.9). Only the contour representations are shown. The position of the waist is given with respect to the entrance aperture. As can be seen, only for aperture-waist distances from 10 to 30 cm the lenses could be tuned such that the transmission exceeds 95%, given the current lens voltage limits. The largest region with transmissions greater than 95% showed the parallel beam. However this beam shape is hardly realizable given the technical circumstances.
In figures 4.10 and 4.11 pictures from simulations with selected lens settings allowing for high transmissions are shown for most of the investigated beams. See [9] for potential

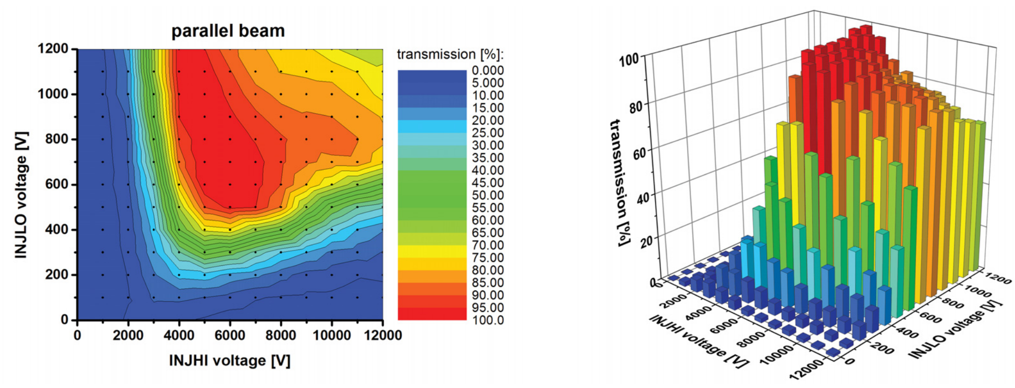

Figure 4.8.: Contour plot and bar diagram representation of the transmission versus the INJHI and INJLO lens voltages for a parallel beam with width 5.3 mm as defined in the text. The injection energy was 50 eV.

contour plots of the cooler injection section.

Figure 4.12 shows exemplary simulations with different injection energies (25 eV and 75 eV) for the beam with waist located 30 cm before the aperture. Only slight differences to 50 eV injection energy are visible, the principal shape is very similar.

To give an idea about the uncertainty of the transmission determined in the simulation, 10 successive measurements were taken for a high and a medium transmission voltage setting. This was done using the beam with a waist 30 cm before the aperture as an exemplary case. For INJHI set to 4000 V and INJLO to 700 V the transmission was $(98.5 \pm 0.3)\%$ and for INJHI set to 1000 V and INJLO to 700 V $(61.0 \pm 1.2)\%$.

To summarize, the simulations suggest that it would be favorable to position the beam waist somewhere between 10 cm and 30 cm from the entrance aperture in order to achieve maximum transmission into the cooler in the new beamline section.

In the simulations presented, space charge effects were not considered. Furthermore the pressure gradient in the cooler tube is unknown, which makes it hard to estimate the amount of buffer gas present in the injection region. Once the ion cooler is operational after having been transferred to VERA, first tests will show to which extent the predictions made for the lens voltage settings with the simulations will accord with experimental observations.

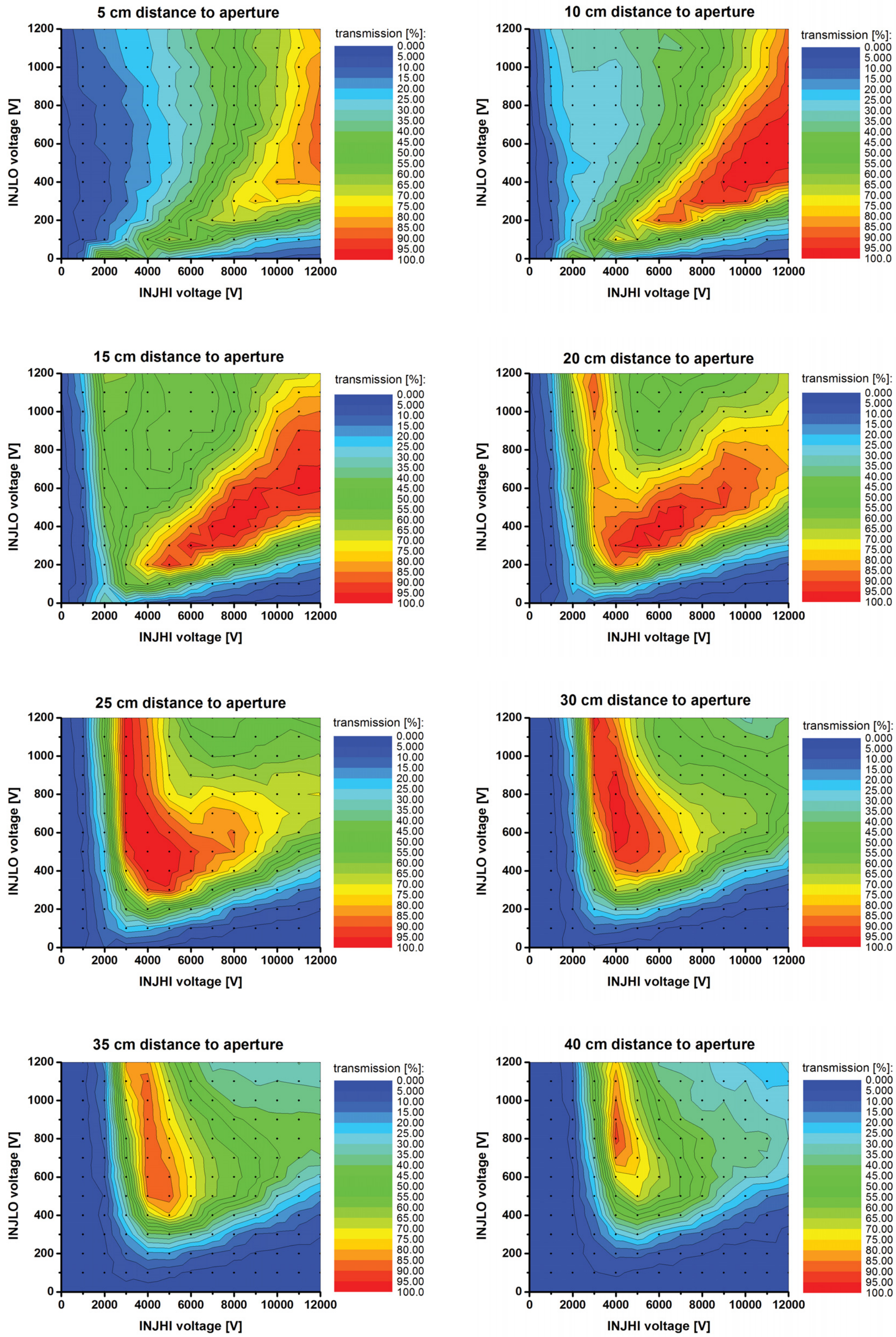

Figure 4.9.: Contour plots of the transmission with respect to the INJHI and INJLO lens voltages for beams with different waist positions. The distance of the waist to the injection aperture is given, where the waist was always located in front of the aperture. The injection energy was kept constant at 50 eV.

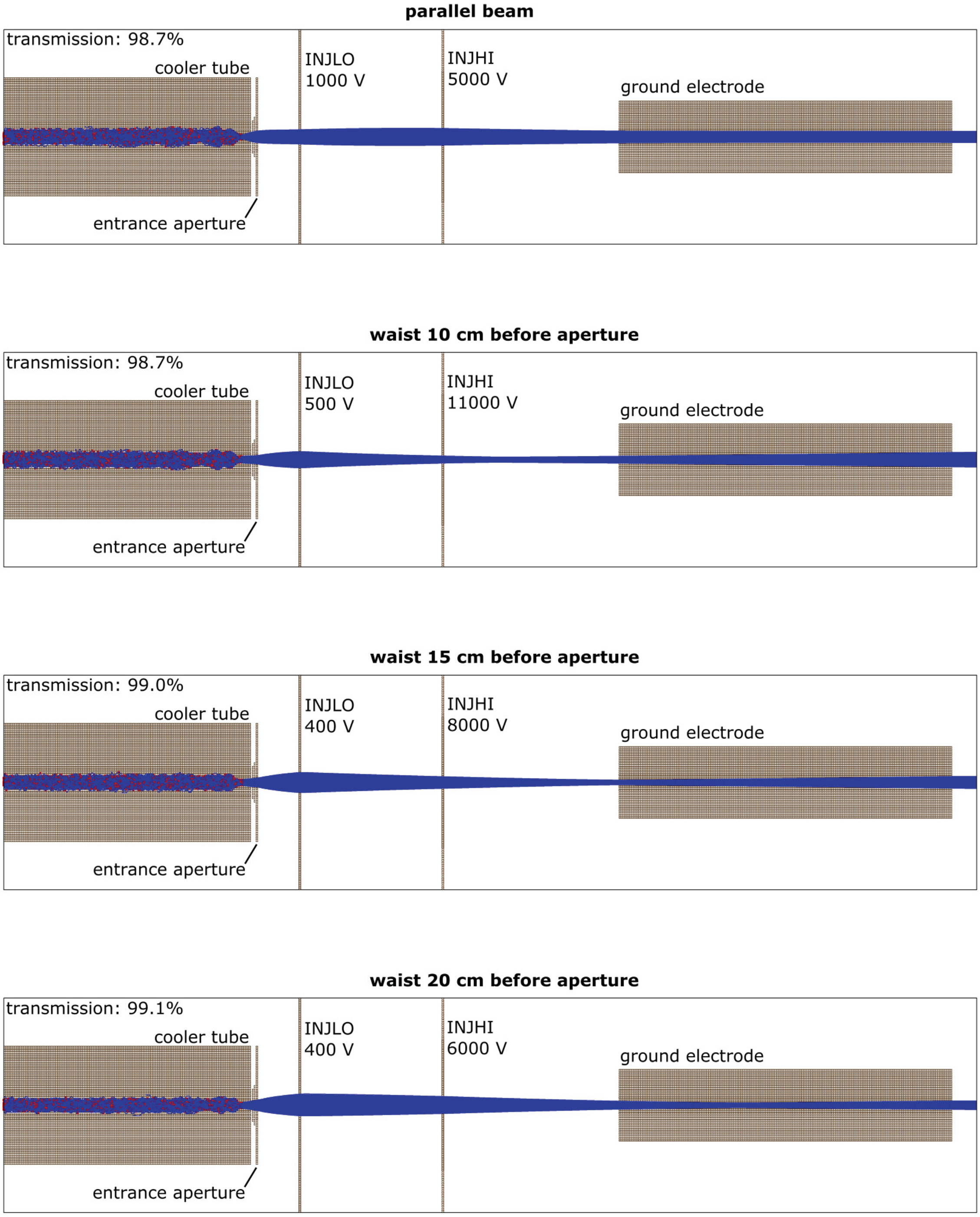

Figure 4.10.: Simulation side views for different beams and chosen lens voltage settings allowing for a transmission above 95%. The red dots in the RFQ indicate collisions of the ions with buffer gas atoms. Not the entire simulation geometry is visible in these illustrations.

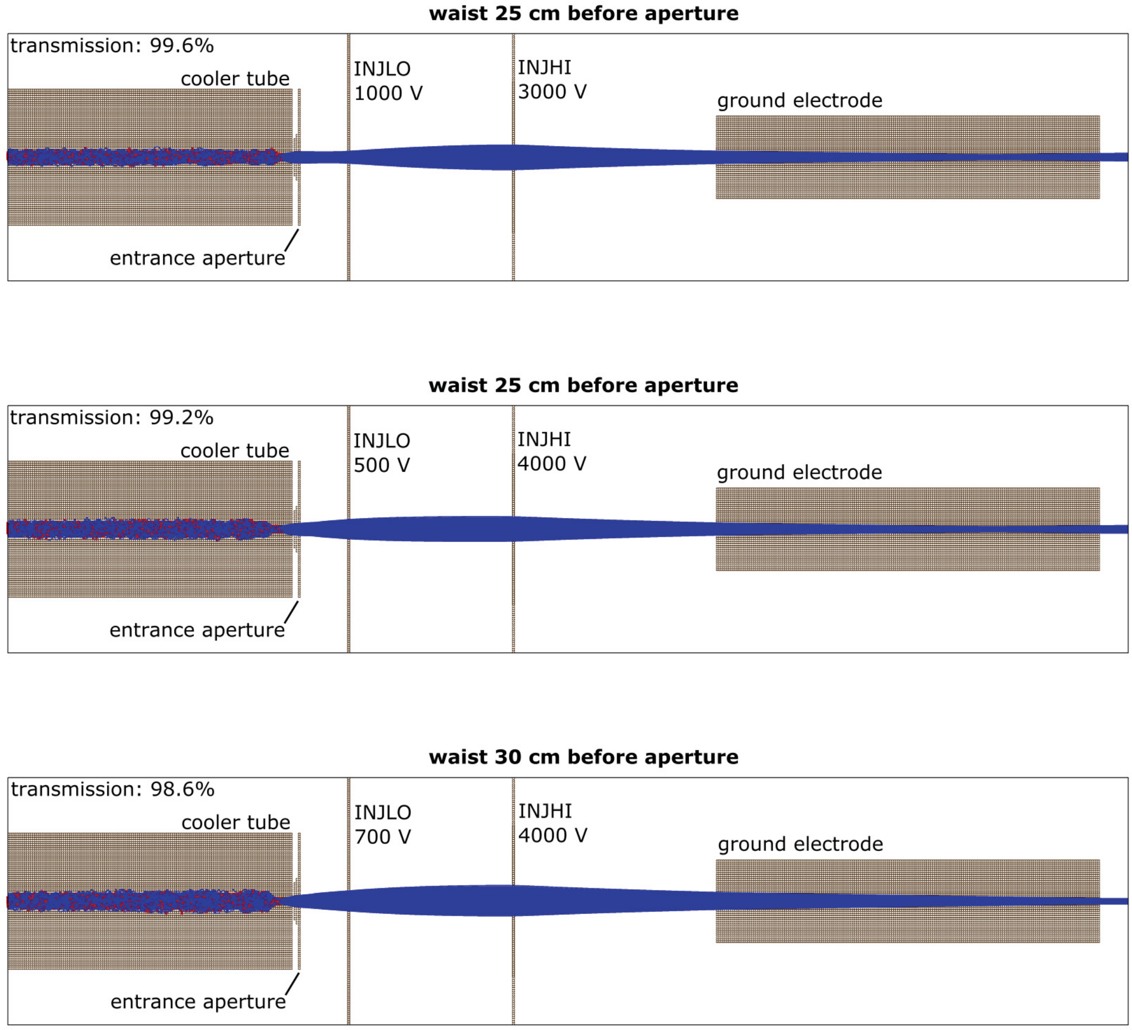

Figure 4.11.: Continuation of figure 4.10. For 25 cm aperture-waist distance two lens settings are shown because the region with maximum transmission in the respective contour plot is quite long, indicating a noticeable difference in the beam shape.

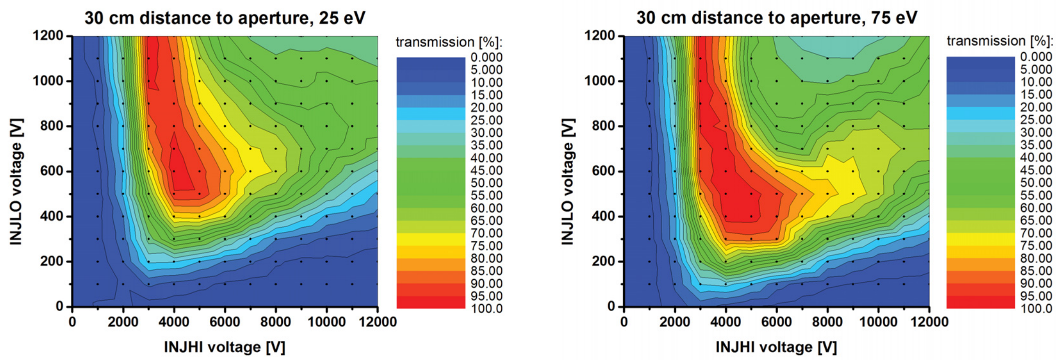

Figure 4.12.: Transmission contour plots for a beam with 30 cm aperture-waist distance for two different injection energies. On the left the injection energy was 25 eV and on the right 75 eV.

4.2.3. Extraction ion optics

The situation on the extraction side of the ion cooler is quite different from the injection side. By buffer gas cooling in the RFQ trapping potential the ion beam is expected to be confined within a distance of 0.5 mm from the central axis [9]. Therefore the transmission through the exit aperture and the lens openings does not present a problem. This was also confirmed by experimental observations with ILIAS, where the ion current measured on the exit aperture practically vanishes when the beam is properly cooled (compare section 5.3). The aim of the following simulations was to get a qualitative understanding of how the EXTHI and EXTLO lens influence the beam shape outside the cooler extraction section. To that end, a beam was started 50 mm inside the RFQ. It was defined more broadly than expected in reality to better visualize the principal beam shaping. The inclusion of buffer gas into the simulation was omitted.

The simulated section ranged from the outer extent of the complete geometry on the extraction side (1248 mm from the reference position in figure 4.7), to 100 mm into the RFQ electrodes (+850 mm from the reference position). Again a grid density of 4 grid units/mm was chosen. This required to thicken the cone of the exit aperture as well as the cone of the EXTLO lens to prevent ions from passing through them (see the geometry file in appendix A.2 for details).
The ions (2000 per run, mass 36, charge -1 e) were started with a filled circle distribution with radius 1 mm positioned 50 mm into the RFQ electrode structure. A filled cone direction distribution with half angle 20° and an initial kinetic energy of 1 eV was used. The injection energy was kept constant at 50 eV. The RF and guide electrode settings were again 2 MHz for a 200 V amplitude and -50 V respectively.

By trying different lens voltage settings some principal observation could be made. The EXTHI voltage limit imposed by the power supply is again 12.5 kV and for EXTLO 1.25 kV. The position of the waist adopted for reasonable settings depends on the lens voltages but most often falls inside the ground electrode (the section going from 24 cm after the exit aperture to 39 cm after the exit aperture). Low EXTHI voltages (up to about 1500 V) and reasonable EXTLO voltages result in a narrow waist and strong angular divergence (see figure 4.13 top). For an EXTHI voltage of for example 2600 V and an EXTLO voltage of 1200 V the waist can be moved as far as roughly 36 cm away from the aperture (see figure 4.13 middle). This distance can be even further increased by increasing the EXTLO voltage beyond the practical voltage limit.
For higher EXTHI lens voltages (for example figure 4.13 bottom, with 5000 V EXTHI and 1200 V EXTLO), the resulting beam is typically much broader at the waist and the waist position falls again within the ground electrode.

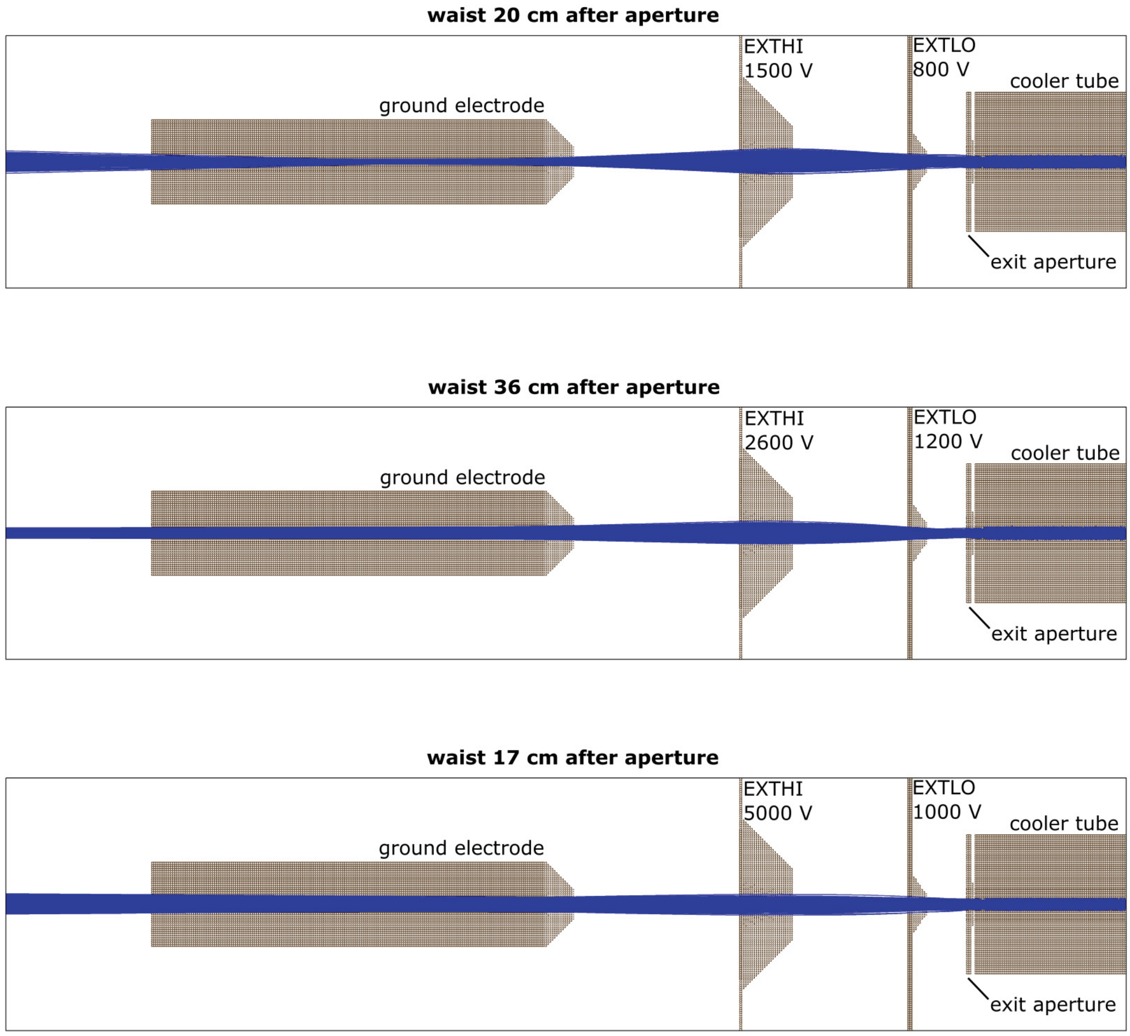

Figure 4.13.: Simulation side views for selected lens voltage settings. A rough estimation of the observed waist position is given for each simulation. The ion direction of flight is from right to left. Not the entire simulation geometry is visible in these illustrations.

5. Measurement results and discussion

Most of the characterization experiments were performed with a $^{63}Cu^{-}$ beam. Copper falls in the mass range that can be handled by the non-resonant RF setup available at that time, the Cu sputter target usually delivered several μA of source output and the ion beam is known to show low contamination at this selected mass. Furthermore with an electron affinity of 1.24 eV it is detachable by a 532 nm laser (2.33 eV) and therefore also well suited to characterize the laser photodetachment suppression capabilities of ILIAS.
$^{127}I^{-}$ extracted from an AgI cathode was also found to be very favorable concerning the source output. Having an electron affinity of 3.06 eV, it cannot be detached by a 532 nm laser. It was used to show that negative ions with an electron affinity higher than the laser energy are not affected by the laser overlap and to test alternative buffer gases (compare section 5.3).

5.1. Transmission

Substantial improvement of the transmission was achieved by the installation of the two compact beam deflectors (see section 4.1) into the beam line cross right after (STEERER2) and right before the cooler (STEERER1), respectively (see figure 3.1). The front deflector was included to allow for a coaxial injection into the cooler and thus to correct for any steering caused by components such as the cooler injection lenses. Without STEERER1 at least 34% of a total ion current of 293 nA in FC1 were always measured on the cooler injection aperture and thus lost. Since the installation of STEERER1, it is possible to tune the setup such that only very little current gets lost on the injection aperture, e.g. less than 10 nA for an ion current of more than 1 μA measured in FC1.
The deflector after the cooler was especially important to correct for a misalignment of the RFQ and associated components which made it very hard to get more than 25% of the extracted beam measured in Faraday cup FC2 through the bender in one of the Faraday cups FC4 or FC5. After the installation of STEERER2 up to 95% of the beam extracted from the cooler could be transmitted to those Faraday cups. The transmission to FC2, however, remained almost unchanged because of the short distance between FC2 and STEERER2.
Additionally, the cooler alignment was slightly improved using a probe laser prior to the measurements presented in the following.

Generally, the transmission was found to strongly depend on the tuning of the setup. Before entering the RFQ cooler, the ion beam has to pass many ion optical components whose control parameters cannot be adjusted independently. A good deal of dedication is required from the operator, since all these adjustments have to be carried out manually.

In the following the transmission through the ion cooler is defined as the ratio of the current measured in Faraday cup FC2 to the current measured in Faraday cup FC1 (see figure 3.1). The ion beam is not trimmed by slits or apertures prior to the detection in Faraday cup FC1, so the entire phase space from the source is focused to the opening of the ion cooler entrance aperture. To avoid an overestimation of the transmission, the beam is tuned into FC1 after the measurement with FC2.
A transmission of maximally 44% of a $^{63}Cu^{-}$ test beam through the ion cooler in full operation was reported in [9]. STEERER2 was already operational at that time. This transmission could be improved to over 60% by the installation of STEERER1 and an additional realignment of the cooler (see figure 5.1).

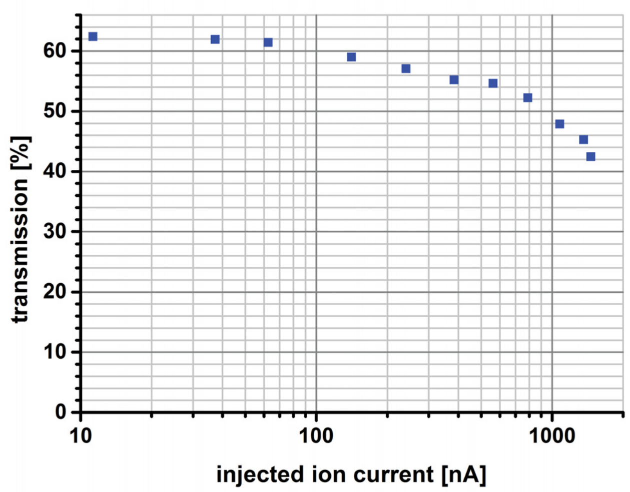

Figure 5.1.: Transmission from FC1 to FC2 versus the injected ion current measured in FC1. The buffer gas pressure was set to 0.16 mbar, the RF frequency to 2 MHz and the RF amplitudes were around 210 V. Above 100 nA a clear drop in transmission caused by space charge effects is visible.

In AMS the current extracted from the ion source at the mass of the trace isotope typically doesn't exceed about 100 nA. As can be seen, the transmission value in that regime is roughly constant above 60%. The transmitted current drops for higher injected currents due to space charge effects. For this experiment the amplitude was set to its maximum around 210 V, further increasing it would have resulted in a shutdown of the RF amplifier because of too much backflow power. Further transmission improvements particularly for the higher currents can be expected by changing from the old non-resonant RF setup to a

newly designed resonant RF circuit, waiting for future operation after the setup will have been transferred to VERA. Test measurements showed amplitudes up to 400 V over the complete required frequency range. The amplitude affects the transmission because the depth of the trapping potential is directly proportional to the RF amplitude (formula 2.6) and therefore an increase should lead to a reduction of space charge losses.
A similar reduction of the beam transmission by space charge effects was observed for positive ion currents at the Spiral-2 High Intensity Radiofrequency Cooler (SHIRaC) at the LPC-Caen laboratory in France [32]. This is one of very few other high intensity RFQs. It is laid out for currents up to 1 μA.

5.1.1. Collisional losses during injection

Before the installation of STEERER1 in front of the cooler entrance, significant beam losses in the injection region were observed and at least partially attributed to collisional losses due to buffer gas leaking from the cooler tube. Liu et al. [18] could significantly improve the transmission of their negative ion RFQ cooler by removing sections of the enclosures surrounding the quadrupole ends. This ensured efficient removal of buffer gas from the injection and extraction region. To see whether also the ILIAS ion cooler could be improved in that way, the tube surrounding its electrode structure was modified accordingly, as already reported in [9]. Large pumping holes were cut out from the tube ends and movable shells were added to allow for a regulation of the pumping hole size and make the changes reversible in case it wouldn't work (see figure 5.2). Before the modifications the gas could leave the cooler tube only through the 3 mm entrance and exit aperture openings, as well as through a 1 mm gap between the aperture and the cooler tube.

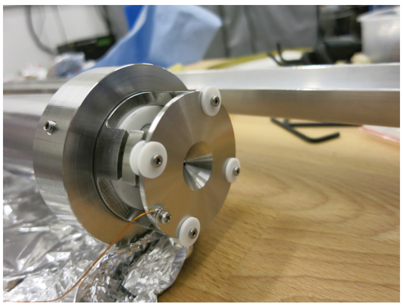

Figure 5.2.: Photograph of the injection side of the cooler tube with the cut out pumping holes and the shell (in open hole position).

The transmission measurement already presented was conducted with the pumping holes fully opened on both ends of the cooler tube. It was repeated for closed pumping holes on the injection side to compare the performance (see figure 5.3). Additionally also the readings of the vacuum measurement cells where compared for the two shell settings (see table 5.1).

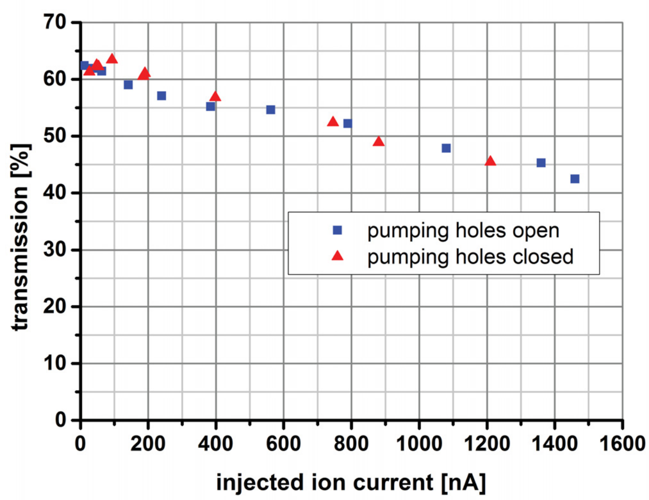

Figure 5.3.: The transmission measurement (figure 5.1) was repeated with the shell closed on the injection side. Again the buffer gas pressure was set to 0.16 mbar, the RF frequency to 2 MHz and the RF amplitudes to around 210 V.

	open shell	**closed shell**
measurement cell	pressure [mbar]	pressure [mbar]
buffer gas inlet	0.16	0.16
front	$8.32{\cdot}10^{-7}$	$8.90{\cdot}10^{-7}$
center	$2.00{\cdot}10^{-5}$	$2.00{\cdot}10^{-5}$
back	$6.04{\cdot}10^{-7}$	$6.10{\cdot}10^{-7}$

Table 5.1.: Pressure values in the cooler beamline section from different vacuum measurement cells for the shell closed and opened. The measurement cells denoted as *front*, *center* and *back* are located near each of the three turbo molecular pumps in the corresponding cooler region displayed in figure 3.2.

No remarkable difference, neither in ion beam transmission nor in the gas leakage to adjacent sections, could be observed. It seems that the buffer gas pressure of typically 0.16 mbar in the middle of the cooler tube drops significantly towards the ends, due to the high flow resistance imposed by the electrode strucure and the electrode holders. It can therefore be assumed that the most relevant region for the buffer gas cooling process is the middle section of the cooler.

With ILIAS in its final state, after all optimizations and the installation of the additional steerers, the collisional losses should be well below 10% of the injected ion current. This estimation is based on experimental experience with the decrease in transmission with rising buffer gas pressure. A further improvement is expected when the cooler is tested with the low emittance beam from the VERA ion source.

5.2. Ion residence time

The main purpose of the ILIAS RFQ ion cooler is to increase the laser-ion interaction time to enable efficient suppression by laser photodetachment. It seems natural to study this aspect directly to gain a better understanding of the underlying interrelations.
SIMION 8.1 simulations suggested a total ion residence time in the ILIAS ion cooler in the order of a few milliseconds [9]. However, the pressure gradient in the cooler tube is unknown and ion-ion interactions (space charge effects) could not be taken into account. To add experimental data to the picture, a simple measurement setup was conceived. The principle idea was to periodically interrupt the ion beam using some fast component located before the cooler while recording the ion current transmitted through the cooler. The distribution of residence times can be obtained from the ion current signal.
Actually there are two ways such a measurement can be realized. Firstly, by recording the ion current's rise while restoring stable beam conditions after a period of interruption, leading to the distribution of residence times while loading the previously empty cooler with ions. And secondly, by recording the ion current's fall while interrupting the ion beam, corresponding to a measurement of the distribution when the cooler in stable operation condition is unloading the ions. Of course the question remains whether either of these two measurement methods properly reflects the residence time distribution under stable conditions. For reasons described in subsection 5.2.4 where the differences between these two methods shall be addressed, the second method (unloading the cooler) was chosen for the measurements that will be presented. All the following subsections, except for subsection 5.2.4, are based on the unloading method.

5.2.1. Experimental realization

First of all a component allowing for periodical interruption of the ion beam had to be found. Naturally the time needed for the stable ion current measured before the ion cooler to completely disappear, had to be far below the residence time that was expected to be in the order of milliseconds. None of the available components of the setup allowed for this time period to be short enough. It was therefore necessary to include an external switch that was fortunately available. This device is based on a fast high voltage transistor switch (HTS 51 from Behlke Power Electronics, Kronberg im Taunus, Germany) and was used to control a preset voltage on one of the electrodes from the electrostatic x-steerer before the magnet (compare figure 3.1). The configuration was such that the ion beam was left on its nominal path while the steerer electrode was on ground potential and was kicked away from it within less than 1 μs from the moment the preset voltage was applied to the electrode. The switch itself was driven by a square wave signal from a function generator which made it possible to average over many successive measurements to suppress the signal noise. Its frequency and duty factor was chosen based on the measured residence

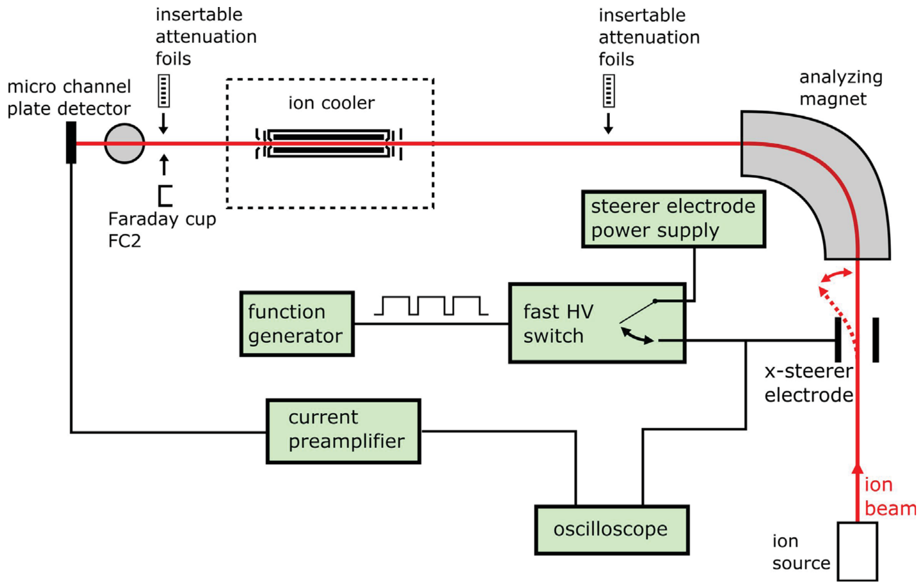

Figure 5.4.: Scheme of the setup for the measurement of the ion residence time. A high voltage switch on a steerer electrode was used to chop the ion beam and the transmitted ion current was recorded with a micro channel plate and a Faraday cup.

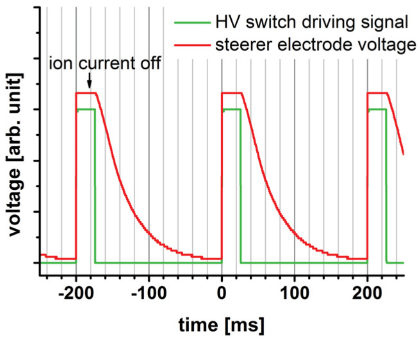

(a) steerer voltage and driving signal

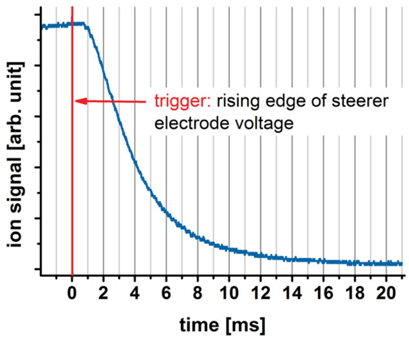

(b) data example

Figure 5.5.: Figure (a) shows the principle steerer electrode voltage progression during a measurement series, as well as the driving signal of the HV switch. Three measurement cycles are visible in the diagram. When the switch closes (at the times -200 ms, 0 ms and 200 ms) the preset voltage is applied to the steerer electrode in less than 1 μs. The plateaus indicate the time during which the ion current from the source is (maximally) deflected away from the cooler and the cooler is unloading the remaining ions. It takes much longer for the deflecting electrode voltage to disappear (and therefore to restore stable beam conditions) after the switch has opened again. This is, however, irrelevant for the residence time measurement.
In figure (b) an example for an averaged ion signal curve is depicted. The steep rise in the steerer electrode voltage in figure (a) sets the oscilloscope trigger. The ion current starts to fall once the minimum residence time is reached. By inverting the curve and differentiating with respect to time, a residence time distribution as presented in subsection 5.2.3 can be obtained.

time. In figure 5.5(a) the progressions of the steerer electrode voltage and the HV switch driving signal during a measurement are shown.
The voltage on the steerer electrode was measured with an oscilloscope (TDS 1002 B from Tektronix, Beaverton, Oregon, USA). Its rising edge served as the start signal for the residence time measurement.
Since also the current dependence was to be investigated, ion currents ranging from 10 pA to several 100 nA had to be measured. A micro channel plate detector was needed for ion currents in the order of 10 pA because the signal from a Faraday cup is to weak to monitor current changes in that regime with a satisfactory time resolution. It was used to amplify the ion current to a few 100 nA measurable on the detector anode. The detector voltage was much lower than the voltage typically applied for count rate measurements and was chosen based on the ion current extracted from the cooler. Prior to being fed into the second channel of the oscilloscope, the ion current signal from the microchannel plate detector was converted into a voltage signal by a low noise current preamplifier (SRS SR570). Figure 5.5(b) shows an exemplary unprocessed data curve obtained with the microchannel plate. The detector was mounted in the beamline cross near the laser entrance window where it replaced Faraday cup FC3. Insertable attenuation foils were installed before the ion cooler and before the micro channel plate detector. They allowed on the one hand to inject very low stable currents and on the other hand to also measure higher currents without changing to the Faraday cup by reducing the current to a manageable amount right before entering the detector.
For ion currents in the order of 100 nA, also a Faraday cup works fine in principle. Nevertheless Faraday cup FC2 was used only for one of the measurements presented in this chapter. Comparative measurements of the residence time distribution for an ion current of several 100 nA injected into the cooler showed that the results obtained with FC2 are consistent with those obtained with the microchannel plate detector.
Again all the experiments were performed with a $^{63}Cu^{-}$ beam and helium buffer gas.

5.2.2. Data evaluation

The averaged current signal curves (e.g. figure 5.5(b)) were inverted if necessary, normalized to the maximum ion current and numerically differentiated with respect to time to obtain distributions of residence times. A subsequent smoothing (weighted moving average algorithm) of the resulting curves was necessary to distinguish the relevant distributions from the noise.
The heights of the presented distributions are arbitrary and carry only relative information. Furthermore the data was not corrected for the time of flight spent in the region outside of the cooler (from the steerer electrode to the cooler entrance and from the cooler exit to the detector). Measurements without trapping potential and cooler high voltage showed that this time is around 40 μs.

5.2.3. Measurement results

Essentially three parameters influencing the ion residence time in the cooler were investigated: the injected ion current, the buffer gas pressure and the strength of the longitudinal guiding field. Each one of them was the object of a series of experiments. The results are presented by showing exemplary plots that illustrate the qualitative relations.

In figure 5.6 ion residence times for different injected ion currents ranging from 32 pA to 460 nA are shown. Clearly the residence time depends strongly on the number of ions in the cooler. For higher currents in the order of 100 nA the mean residence time is some 100 μs. It seems that a field gradient is built up by the accumulated space charge, that is proportional to the amount of charge. This results in much shorter residence times for higher ion currents. Compared to just tens of pA of injected ion current, the average residence time for more than 100 nA of injected current is more than an order of magnitude shorter.
For an ion current of 32 pA the residence times are smeared out over a very large time range, reaching up to 100 ms. This suggests that in that regime the drift to the cooler exit is to a greater extent governed by random diffusion in the buffer gas. The same behavior is present for different buffer gas pressures, with a shift to smaller residence times for smaller buffer gas pressures, as will be addressed shortly.
There seems to exist only very little published literature treating the residence time in buffer gas filled RFQ coolers for high intensity ion beams (order of 1 μA). In [33] the residence time in a positive ion cooler for injected ion currents from 0.25 nA to 1.02 nA is treated. Also there a similar behavior could be observed, but of course on a smaller scale.

In a next step the dependence of the residence time on the pressure of the buffer gas was investigated. With higher pressure the ions thermalize less far into the cooler due to the greater number of random collisions with the gas atoms. This results in a longer distance to the cooler exit that the ions have to cover by diffusion in the buffer gas. One would therefore expect longer residence times for higher buffer gas pressures. In figure 5.7 distributions are shown for different gas pressures ranging from the optimum for cooling a $^{63}Cu^-$ beam of about 0.16 mbar (compare section 5.3) to 0.30 mbar. The measurements were conducted for 340 nA, 3.2 nA and 32 pA injected ion currents. An increase in the minimum residence time for higher buffer gas pressures is observed in all three current regimes. However, it is clear that the influence of the buffer gas pressure on the residence time is much smaller than that of the injected ion current.
In linear scale the asymmetry of the distributions becomes more apparent. Most ions leave the cooler not long after the respective minimum residence time, followed by a large tail of ions with longer residence times. This might be explainable by ions of which the forward

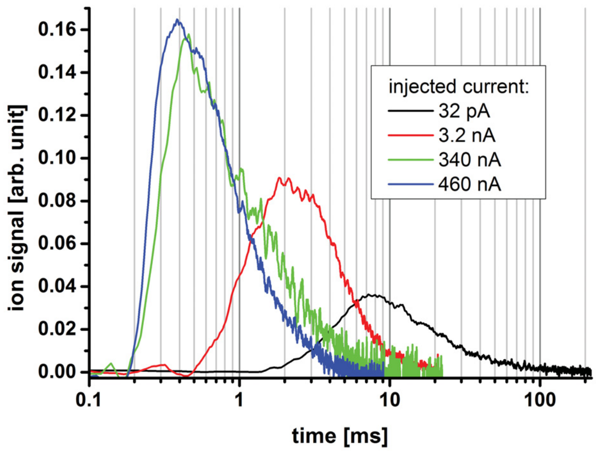

Figure 5.6.: Distribution of residence times during cooler unloading for different injected ion currents. During the experiment the guiding field strength was 2.2 V/m and the buffer gas pressure 0.30 mbar. For the distribution at 460 nA Faraday cup FC2 was used instead of the microchannel plate detector. To allow for a reasonable presentation, some of the distributions had to be rescaled vertically.

momentum was significantly reduced by head-on collisions with gas atoms, possibly even leading to them being temporarily directed opposite the beam direction. The residence time of ions that are spared from these severe collisions is expected to be near the minimum residence time. Moreover, a contribution to these tails may again come from the space charge potential gradient in the cooler, which decreases with the number of ions leaving the cooler.

In principle a shorter residence time is expected with increasing the guiding field strength. To give an idea, simulations revealed that the overall potential difference between the cooler ends that is generated by the guiding electrodes is a few volts for typical settings [9]. When tuning the ILIAS components for currents of several 100 nA, hardly any difference in the transmitted current or any other parameter can be observed when the voltage on the guiding electrodes is changed over a range of several 100 V. This is also confirmed by the distribution of residence times for an injected ion current of 460 nA (figure 5.8 top). No significant difference is observed between 2.2 V/m, 6.6 V/m and 11.0 V/m guiding field strength. It seems that the space charge potential gradient by far exceeds the gradient generated by the guiding electrodes.
The measurement was also conducted for 3.2 nA and 32 pA injected ion currents. Only for 3.2 nA a clear influence of the guiding potential can be observed (see figure 5.8 middle for an exemplary diagram). The distribution is squeezed on the right side, meaning that the tail of ions spending the longest time in the cooler is shifted towards smaller residence times because of the greater guiding potential. However, it is not obvious why

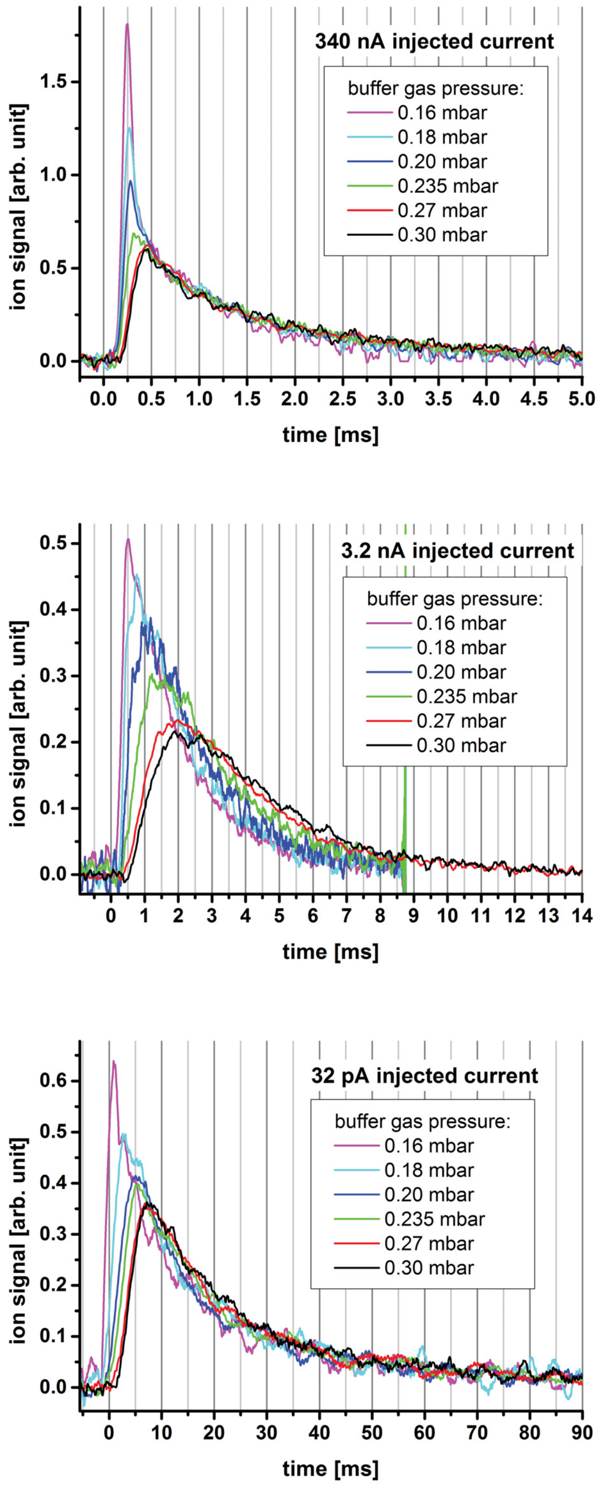

Figure 5.7.: Residence time distributions during cooler unloading for different buffer gas pressures for 340 nA (top), 3.2 nA (middle) and 32 pA (bottom) injected ion currents. The guiding field strength was 2.2 V/m. Note the differences in time range for different ion currents.

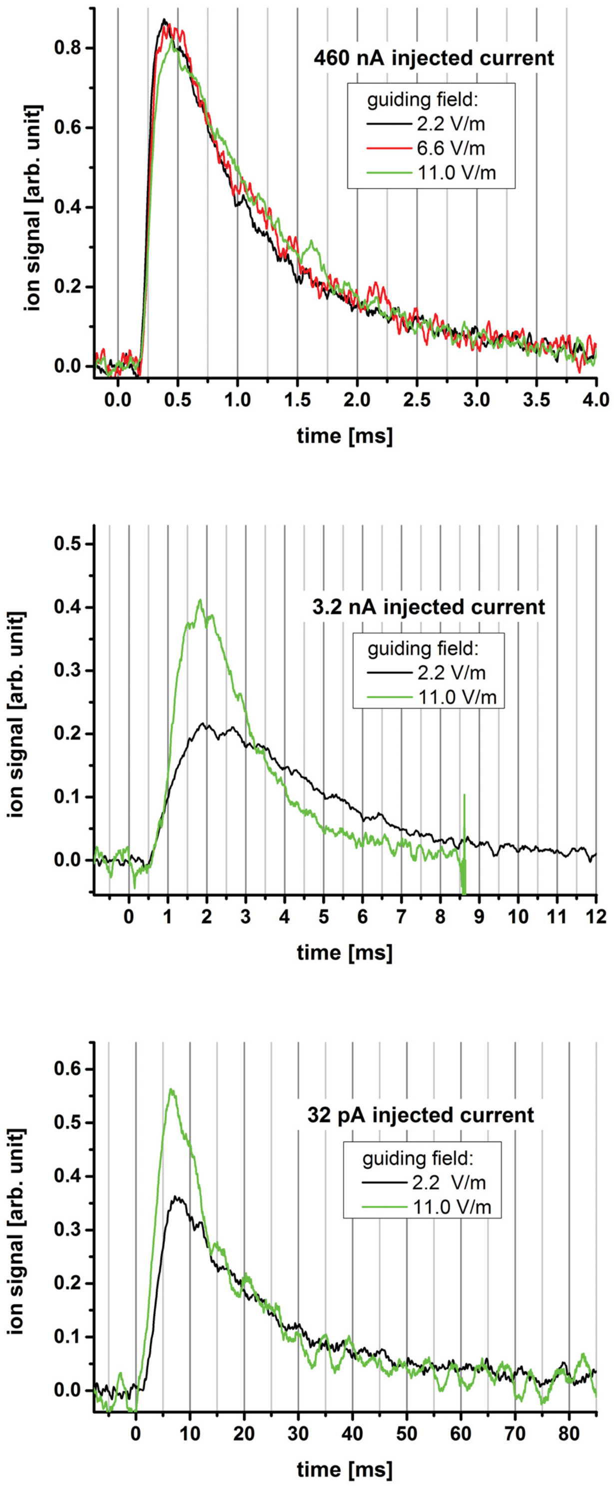

Figure 5.8.: Residence time distributions during cooler unloading for different guiding electrode voltage settings for 460 nA (top), 3.2 nA (middle) and 32 pA (bottom) injected ion currents. The buffer gas pressure during the experiment was 0.30 mbar. For practical reasons the distributions shown in the top diagram were obtained using Faraday cup FC2 instead of the microchannel plate detector. Again note the differences in time range for different ion currents.

this shouldn't also have an effect on the minimum residence time and hence on the left side of the distribution. It could be that the guiding field is mainly relevant for those ions moving temporarily opposite to the beam direction.

5.2.4. Loading effects

As mentioned in the introductory section the residence time measurement can also be carried out by recording the ion current's rise while restoring stable beam conditions after a period of interruption, leading to the distribution of residence times while loading the previously empty cooler with ions. The measurement setup is very similar to that in figure 5.4, only some rearrangements concerning the steerer electrodes and their power supplies are required. Interestingly the residence time distributions obtained with this method point to some odd behavior. In figure 5.9 exemplary distributions for both methods are shown.

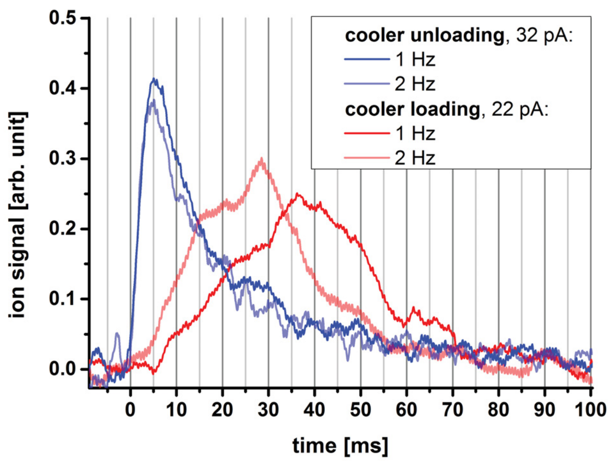

Figure 5.9.: For ion currents of 32 pA and 22 pA, distributions obtained with both measurement methods and two different frequencies of the driving signal are plotted. The designation *cooler unloading* refers to the method used to do the experiments that were presented in the previous subsection, *cooler loading* to the alternative. The buffer gas pressure was 0.20 mbar and the guiding field strength 2.2 V/m throughout.

Not only are the distributions obtained with the alternative method strangely shaped for many settings of the parameters under investigation, but also the residence time is found to depend on the frequency of ion beam chopping. Whether this points to some charging phenomenon in the ion cooler or indicates a problem with the measurement setup will have to be further investigated.

Using this method, the minimum residence time was observed to be greater than in the measurements presented in the previous subchapter. This makes sense, since the first ions entering the cooler are not affected by the space charge potential gradient that has yet to build up. Ergo equilibrium conditions should not be well reflected at the beginning. With the other measurement method, where the ion current is interrupted by the steerer, the situation is different. Here equilibrium conditions should be well reflected at the beginning. This and the absence of the strange effects described above are the reasons why the *unloading* method was chosen to study the ion residence time.

5.3. Buffer gas cooling and photodetachment experiments with test isotopes

The significant improvement of the beam emittance by buffer gas cooling can be demonstrated experimentally with ILIAS by measuring the ion current detected with the exit aperture while varying the buffer gas pressure. Since the beam should be well confined to a narrow region around the central axis, the transmission through the exit aperture (opening with 3 mm diameter) should increase. This can be clearly observed by a decrease in the current measured on the aperture. Thereby the overall transmission through the cooler increases. In figure 5.10 the results from such an experiment are shown.

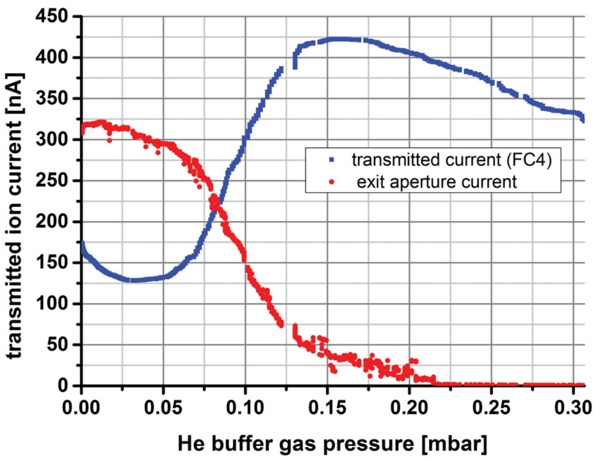

Figure 5.10.: $^{63}Cu^{-}$ ion current detected in Faraday cup FC4 and on the cooler exit aperture vs. the helium buffer gas pressure. As the ion beam gets more confined to the central axis, the current on the aperture drops severely.

Again a $^{63}Cu^{-}$ test beam was used. The current lost on the exit aperture practically vanishes for helium buffer gas pressures above 0.20 mbar.
The transmitted ion current (measured in FC4) shows a maximum for about 0.16 mbar. Factors contributing to the decrease for pressures higher than the optimum might be the occurrence of more scattering inside the ion cooler and increased collisional detachment losses in the entrance region.

In the ILIAS laboratory also argon and nitrogen are available. Both were tested as alternative buffer gases. To that end the transmitted ion current vs. the buffer gas pressure was recorded for argon, helium and nitrogen (figure 5.11). For this experiment a $^{127}I^{-}$ test beam was used. Initial currents without gas ranged from 400 nA to about 450 nA. Beside some instabilities during the experiment, helium quite clearly presents the most favorable choice. This accords with experimental experience and results from simulations

[24, 34, 35]. The transmission for helium has an optimum at about 0.07 mbar. For the other gases the transmitted ion current never exceeds the initial current. Only a plateau at about 200 nA appears in case of nitrogen. This is rooted in the mass of the gas atoms. The energy transfer to the ions is higher in collisions with the heavier argon atoms or nitrogen molecules. Subsequently the probability that collisions lead to neutralization or ions leaving the trapping potential also increases.

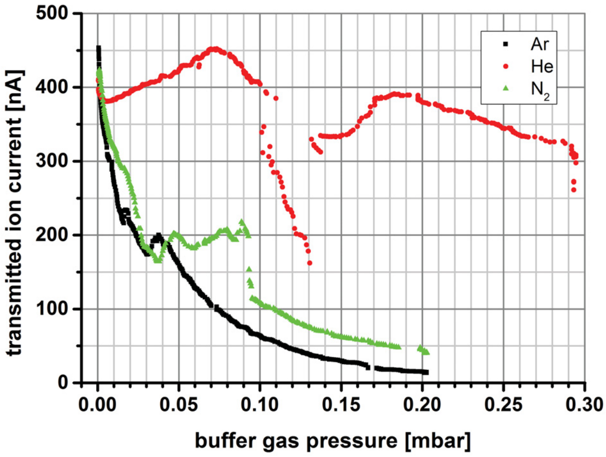

Figure 5.11.: Transmitted $^{127}I^-$ current vs. buffer gas pressure for argon, helium and nitrogen.

The lengthening of the ion-laser interaction time by buffer gas cooling, together with the constraint of the ion beam to the region of interaction, should result in an increase of the suppression by laser photodetachment with rising buffer gas pressure. For experimental verification the negative ion current in Faraday cup FC4 was measured for different buffer gas pressures (figure 5.12). This was done once without the laser and once with the laser at maximum power (10.8 W transmitted to the power meter behind the magnet) overlapping the negative ion beam. As expected, the suppression by laser photodetachment rises with the buffer gas pressure. At a pressure of 0.25 mbar or higher the transmitted ion current is lowered by more than five orders of magnitude compared to the corresponding current without laser overlap. This is however only a lower limit. ILIAS completely lacks the means for ion species identification. The actual suppression might be even higher but escapes demonstration due to a background from a different ion species which is not detachable by a 532 nm laser. Once the full detection capability of VERA will be available to analyze the beam extracted from the cooler, the actual suppression limit can be determined.

A suppression factor can be defined as $\frac{n}{n_0} = e^{\sigma\phi t}$ with the number of ions n, the initial ion number n_0, the photodetachment cross section σ, the photon flux ϕ and interaction time t. This coincides with the inverse ratio of the left side of equation 2.2. The laboratory

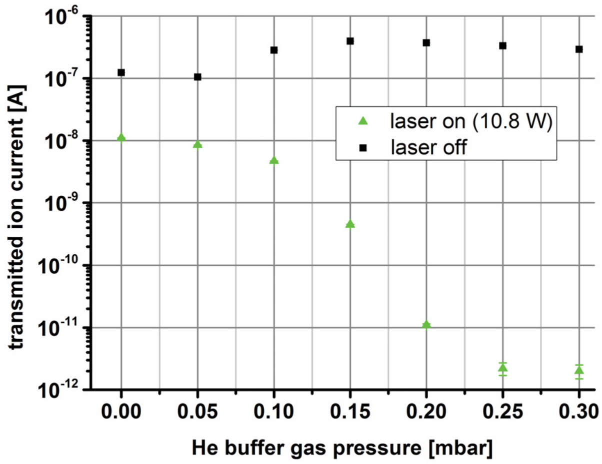

Figure 5.12.: The $^{63}Cu^{-}$ ion current in FC4 after the cooler vs. the helium buffer gas pressure was measured once without the laser and once with the laser at maximum power overlapping the ion beam. 10.8 W of the nominal 18 W laser power were transmitted to the power meter behind the magnet. The current uncertainties are mostly smaller than the plotted symbols.

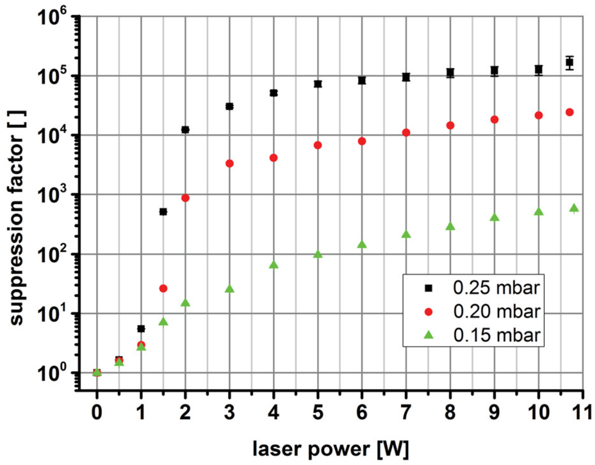

Figure 5.13.: Suppression factors versus laser power for three different helium buffer gas pressures (0.15 mbar, 0.20 mbar and 0.25 mbar). At 0 W ion currents were 390 nA at 0.15 mbar, 340 nA at 0.20 mbar and 330 nA at 0.25 mbar. The suppression factor uncertainties are mostly smaller than the plotted symbols. The laser power was measured as usually behind the magnet after the laser beam exited the beamline.

equivalent would be the ratio of the transmitted ion current without laser overlap to the transmitted ion current with laser overlap. Under the assumption that the cross section and the interaction time are constant, the suppression factor should follow an exponential behavior as a function of the laser power (photon flux). This is clearly not the case when looking at the data in figure 5.13, where experimentally determined factors are plotted for

three different He buffer gas pressures.
An attempt for a qualitative explanation can be made when considering the dependence of the ion residence time, and therefore also the ion-laser interaction time, on the injected ion current. This was discussed in section 5.2 in greater detail. A threshold is visible at about 1 W where the suppression starts to shoot up, especially for 0.20 mbar and 0.25 mbar. It seems that at this laser power the ion current in the cooler and therefore also the space charge density is reduced enough by laser photodetachment to result in a significantly longer residence time of the remaining ions (compare figure 5.6). This leads to a more efficient suppression, again reducing the current, and so forth.
A second contribution to the deviation from the exponential behavior could come from contamination in the copper beam coming from ions that are detachable by a 532 nm laser but have a different photodetachment cross section. Meaning that, in mathematical terms, the cross section in formula 2.2 is itself a sum of the cross section of copper and of the hypothetical contaminating ion species. However, because of the low level of contamination expected in a copper beam, this effect should be small in comparison.

The suppression capability of ILIAS was also characterized in a different way. The ion current transmitted into Faraday cup FC4 was recorded while switching the laser on and off in intervals of 15 s. This was done for a $^{63}Cu^-$ and a $^{127}I^-$ beam (figure 5.14).
The electron affinities of Cu and I are 1.24 eV and 3.06 eV respectively [26]. Again the suppression by more than 5 orders of magnitude can be observed for $^{63}Cu^-$.
The effect of laser photodetachment on a beam of ions with an electron affinity of more than 2.33 eV (532 nm laser) was studied by changing to an iodine cathode and repeating the very same experiment. The $^{127}I^-$ ion current is clearly not affected by the laser overlap (figure 5.14 bottom), which demonstrates the selectivity of the filtering technique.

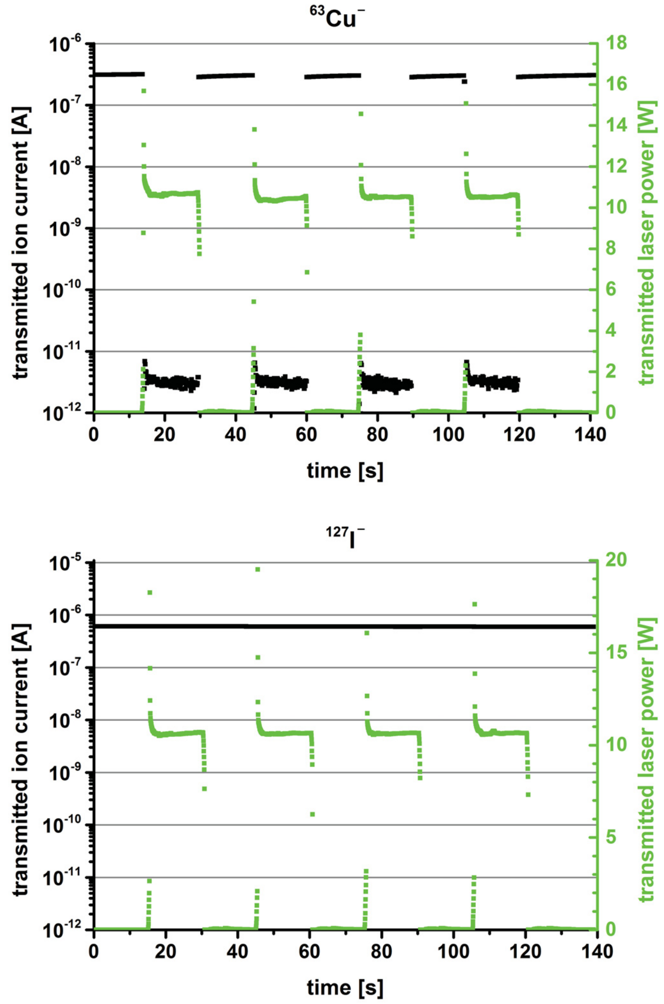

Figure 5.14.: Detachment study at 0.16 mbar buffer gas pressure with a $^{63}Cu^{-}$ (top) and a $^{127}I^{-}$ (bottom) beam. Copper with an electron affinity of 1.24 eV is suppressed by more than 5 orders of magnitude in the intervals with the laser switched to maximum power. Iodine with an electron affinity of 3.06 eV is unaffected by the laser overlap. The overshoot of the laser power curve is mainly an artifact of the laser power meter.

5.4. MgO^- and AlO^-

AMS measurements of ^{26}Al suffer from a poor ion source performance when extracting $^{26}Al^-$ from a sputter ion source. Using the molecular form $^{26}Al^{16}O^-$ instead leads to a current output improvement by more than a factor of 10 [36] and therefore shorter measurement times and better sensitivities. But while the stable isobar ^{26}Mg doesn't form negative ions, the molecule $^{26}Mg^{16}O^-$ does form and limits the measurement sensitivity of this alternative method. Separation of ^{26}Mg from ^{26}Al on the high energy side is possible at large AMS facilities by careful chemical treatment of the sample and the use of a gas filled magnet to distinguish by different energy loss characteristics and mean charge state in matter [37]. A potential alternative applicable to AMS facilities of any size would be to use suppression by laser photodetachment to purify the ion beam in the injector stage. With an electron affinity of 1.62 eV [38], MgO^- is detachable by a 532 nm laser (2.33 eV) as opposed to AlO^- with an electron affinity of 2.60 eV [26]. Hence this presents a wonderful opportunity to directly study a first potential application for AMS using the test setup ILIAS.

5.4.1. Buffer gas cooling and laser photodetachment of AlO^-

A copper cathode filled with Al_2O_3 was used as a sputter target. The experiments were performed with the molecule $^{27}Al^{16}O^-$. Currents up to 1.05 μA at mass 43 u could be extracted from the source. A maximum transmission of about 30% into Faraday cup FC4 was reached for a 1 μA current. The reason for this slightly lower transmission compared to $^{63}Cu^-$ (compare section 5.1) remains to be explored. As was already shown for $^{63}Cu^-$ the transmission of AlO^- increases with buffer gas pressure as cooling sets in, while the current measured on the exit aperture decreases due to the longer ion-laser interaction time and the confinement of the ion beam to the interaction region (see figure 5.15).
AlO^- with an electron affinity of 2.60 eV is not detachable by a 532 nm laser (2.33 eV). Again an experiment was conducted switching the laser on and off in intervals of 15 s while recording the transmitted ion current (figure 5.16). Unlike in the case of $^{127}I^-$, the presumable AlO^- current is reduced by about 3% by laser photodetachment. It is likely that this reduction is caused by the presence of a contaminating ion species with an electron affinity lower than the laser energy. A clear answer will have to wait for future steps of the project. With ILIAS the ion beam extracted from the cooler cannot be analyzed with respect to the ion species composition. Only once the full isotope analysis capabilities of VERA will be at hand, the origin of the 3% mass 43 u current that was photodetached can be explained.

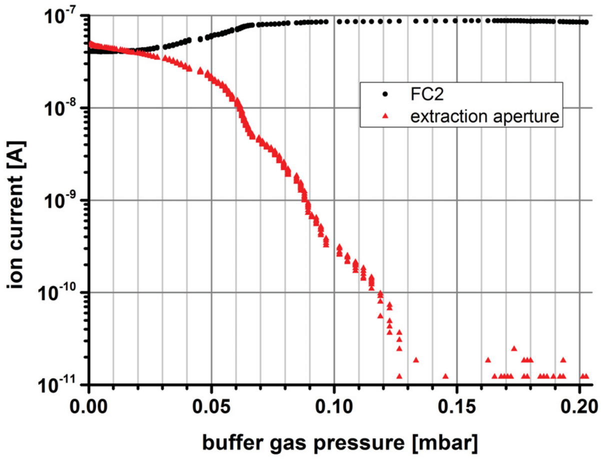

Figure 5.15.: The ion current at mass 43 in Faraday cup FC2 and on the exit aperture was measured while varying the gas pressure. With rising pressure the transmission increases and the current on the exit aperture decreases due to the axial confinement by buffer gas cooling. The sensitivity setting of the current preamplifier (SRS SR570) connected to the exit aperture is in this case inadequate for currents below about 20 pA.

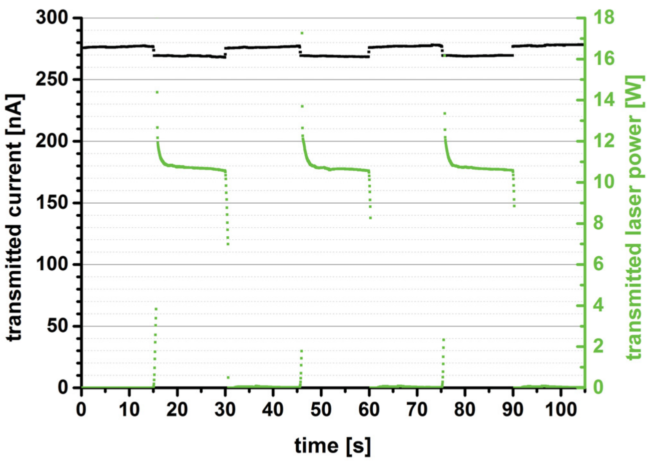

Figure 5.16.: Photodetachment study of $^{27}Al^{16}O^-$. The laser was switched on and off in 15 s intervals. The slight reduction of the ion current measured in FC4 by about 3% in the periods with laser overlap most likely comes from contamination from ion species with an electron affinity of less than 2.33 eV.

5.4.2. Buffer gas cooling and laser photodetachment of MgO^-

Magnesium has three relatively abundant isotopes: ^{24}Mg (78.99%), ^{25}Mg (10%) and ^{26}Mg (11.01%) [36]. For the following experiments a MgO filled Cu cathode was used and the most abundant molecule at mass 40 u ($^{24}Mg^{16}O$) selected. Firstly the transmission dependence on the buffer gas pressure was investigated. When recording the ion current transmitted into Faraday cup FC4 versus the buffer gas pressure, something unexpected was observed (figure 5.17).

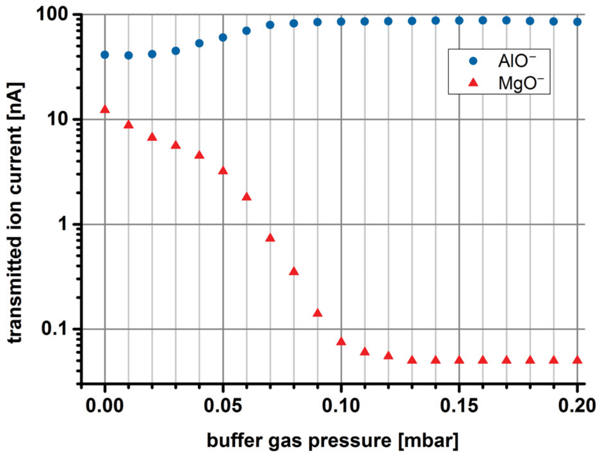

Figure 5.17.: MgO^- and AlO^- current transmitted into Faraday cup FC2 vs. the helium buffer gas pressure.

Unlike the AlO^- current, the MgO^- current droped with rising gas pressure. Exposing the MgO^- beam to the helium in the RFQ lowered the current by a factor of about 250 with respect to the ion current at 0 mbar. No obvious reason comes to mind that could explain this behavior. The electron affinity of Mg is 1.62 eV. In order to rule out collisional detachment as the main cause, the influence of the injection energy on this behavior was investigated. Figure 5.18 shows scans of the cooler high voltage determining the injection energy for AlO^- and MgO^-.
As already explained in section 3.2.1 the optimum injection energy can be understood as a trade off between the increase of collisional detachment losses for higher injection energies and the increase in angular divergence for lower injection energies. For AlO^- an optimum is found at about 35 eV. In case of MgO^- an optimum can be expected at about 22 eV. However, again the beam is shown to be more suppressed with increasing buffer gas pressure, independent of the injection energy.

Figure 5.19 shows detachment experiments at 2 W transmitted laser power for three different buffer gas pressures. Clearly the suppression factor increases with the buffer gas pressure. The suppression factor is roughly 6 for 0.075 mbar, 20 for 0.10 mbar and 50 for 0.20 mbar. This increase is what would be expected if the MgO^- beam were actually cooled in the RFQ. The underlying reason for the big losses by cooling are unclear and will have to be further investigated.

To verify the element selective suppression of MgO^- and to emphasize that it is not

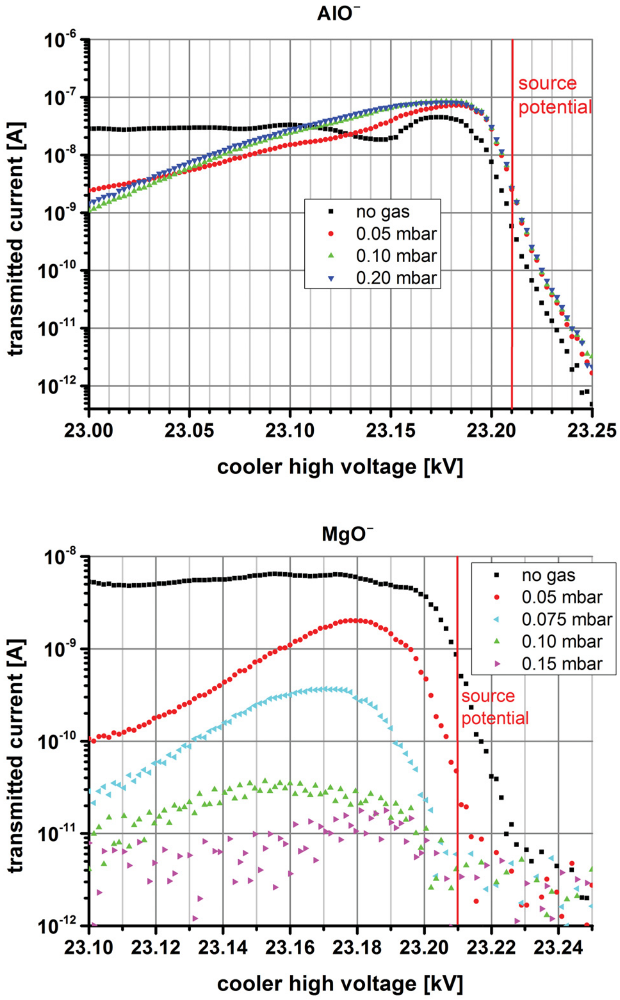

Figure 5.18.: Transmitted AlO^- (top) and MgO^- (bottom) current vs. the injection energy for various buffer gas pressures. The injection energy is determined by the difference between the cooler high voltage platform potential and the ion source potential (cathode voltage + additional acceleration). In the diagrams a cooler high voltage of for example 23.20 kV would correspond to an injection energy of 10 eV.

caused by poor tuning of the machine, another experiment was conducted. Using a mixed sputter target material (Al_2O_3 + MgO + ^{35}Cl enriched AgCl + Cu) the ion beam was mass analyzed before the cooler with Faraday cup FC1, as well as after the cooler with FC4 with and without laser overlap. The three resulting mass scans were then compared to analyze the effect of buffer gas cooling and laser photodetachment on the ions the beam is composed of. Chlorine added control peaks to the spectrum to verify that the transmission doesn't change substantially when leaving the mass region of AlO and MgO without retuning the setup.

Again the suppression by buffer gas cooling is observable (figure 5.20). In contrast to Cl^- and AlO^-, the MgO^- peaks were reduced inside the cooler to a greater extent than can

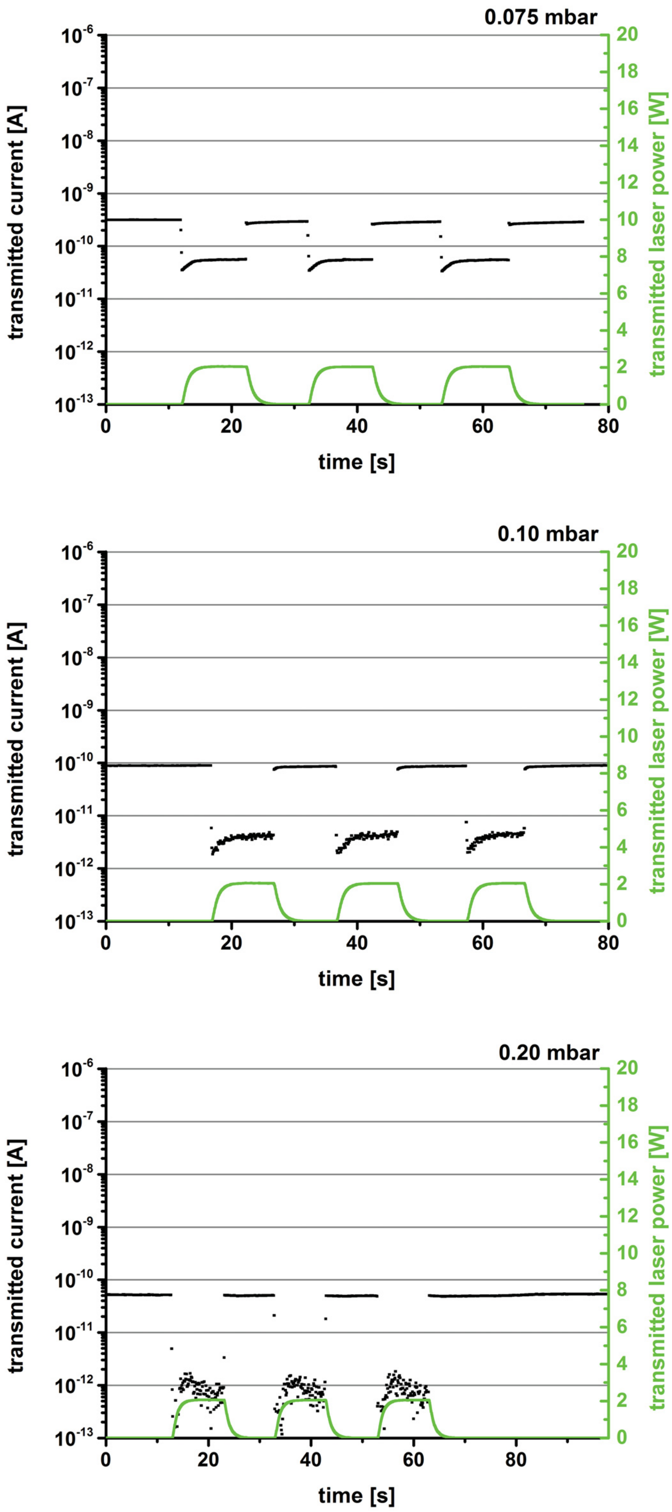

Figure 5.19.: MgO^- detachment at 2 W transmitted laser power for 0.075 mbar (upper), 0.10 mbar (middle) and 0.20 mbar (bottom) buffer gas pressure. The relative suppression is greater for higher buffer gas pressures, which leads to the conclusion that the MgO^- ions are slowed down by buffer gas cooling.

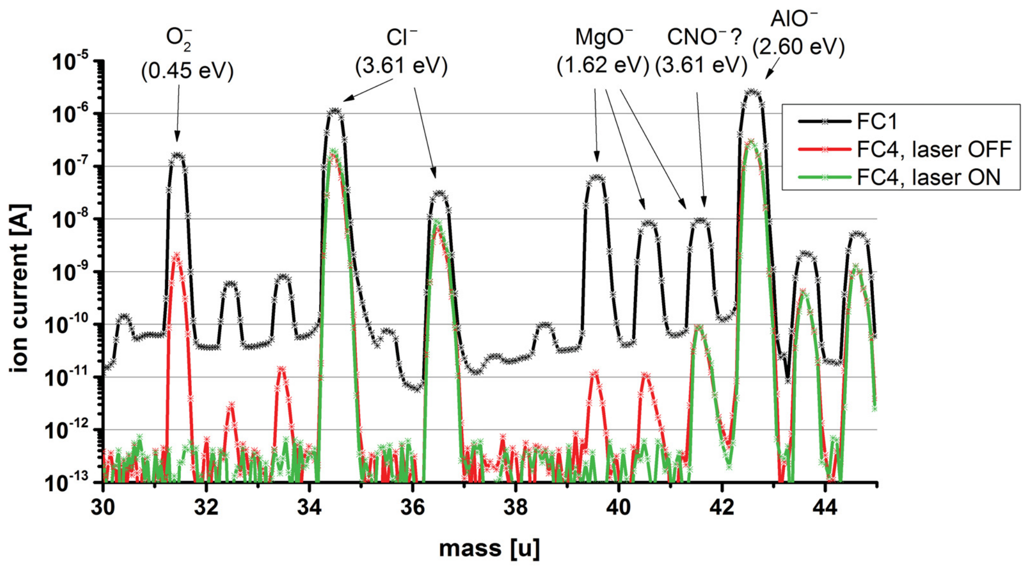

Figure 5.20.: Mass scans from a copper cathode filled with a mixed material (Al_2O_3 + MgO + ^{35}Cl enriched AgCl). For the scans in FC4 the buffer gas pressure was 0.20 mbar. The maximum transmitted laser power was 10.8 W. Only the relevant peaks are labeled, with the respective electron affinities noted in brackets (values taken from [26, 38]). The significant decrease in height of the Cl^- and AlO^- peaks is explained by the poor transmission through the cooler that went along with this experiment. It was that poor because the spectrometer and the RFQ cooler could not be optimized for each specific mass during the scans.

be explained by the limited transmission. The obvious decrease in peak height for the Cl^- and AlO^- peaks was caused by the poor transmission through the cooler. The transmission was significantly less than the maximum transmission described in chapter 5.1, since both the spectrometer and the RFQ cooler were not optimized for a specific mass but for a quite broad mass range. Retuning of the setup for each mass during the scans would have been too time-consuming with respect to ion source stability.

O_2^- with an electron affinity of 0.45 eV is suppressed more strongly than Cl^- and AlO^- by going through the cooler, but the relative suppression still is stronger for MgO^-. A low electron affinity doesn't seem to be the reason for the suppression of MgO^- by buffer gas cooling. With the laser overlapping the ion beam on maximum power (10.8 W) all peaks with molecules or elements with an electron affinity of less then 2.33 eV vanish.

6. Conclusions and outlook

The main aims of this thesis were to improve the transmission through the RFQ ion cooler, to characterize the setup with respect to buffer gas cooling and suppression by laser photodetachment, to study the suppression of MgO^- relative to AlO^- and to measure the ion residence time in the cooler. Summarizing, all of them were met. The ion beam transmission through the RFQ ion cooler was substantially improved by the installation of two novel compact beam deflectors that were constructed as a part of this thesis project. STEERER1 reduced the losses on the entrance aperture and STEERER2 improved the transmission from the cooler extraction to the Faraday cups FC4 and FC5. A competitive transmission through the cooler above 60% was achieved for a $^{63}Cu^-$ test beam of a few nA. This value was found to decrease with the amount of injected current due to space charge effects. Over all more than 1.4 μA could be extracted from the ion cooler during this experiment. Improvements with respect to space charge effects are expected by using a newly designed resonant RF setup already available.
A suppression by more than five orders of magnitude by laser photodetachment was shown for a $^{63}Cu^-$ test beam using a 532 nm laser. A MgO^- beam could be suppressed by four orders of magnitude. This has potential to improve AMS measurements of ^{26}Al. The underlying reason for the revealed suppression of MgO^- by buffer gas cooling alone, will have to be further investigated.
Comprehensive measurements provided a clearer picture on the ion residence time inside the RFQ. Above all, a strong dependence on the injected current was observed. Residence times in the order of 100 μs for several 100 nA and in the order of 10 ms for several 10 pA injected currents were measured.
It can be concluded that the ILIAS negative ion cooler now is able to perform at least as well as similar existing negative ion coolers.

The fulfillment of the main design requirements and the successful completion of the test measurements paved the way for the next step of the ILIAS project. The coupling of the setup to VERA is already ongoing. ILIAS has been disassembled and the relevant components transported to the accelerator hall. The beamline section of VERA connecting Source2 in figure 1.1 was extended to accommodate the laser photodetachment filtering system. The cooler section including STEERER1 and STEERER2 of ILIAS was transferred basically unchanged.

In the new beamline section an ion source with a large target wheel will allow for fast and comfortable sample change, as opposed to the single cathode source of ILIAS. This will allow for fast switching between ion beams of various target materials. The extracted ion beam is mass preselected by a 90° magnet whose chamber can be supplied with a high voltage to alternate electrostatically between the mass of the trace isotope of interest and that of the stable reference isotope for isotopic ratio measurements. The obtained results concerning the residence time in the cooler, especially about the loading effects, will have to be taken into consideration for the establishment of measurement schemes.
An electrostatic analyzer will direct the ion beam extracted from the cooler away from the axis of laser-ion interaction.

Since VERA offers many possibilities to discriminate between different ion species, soon the actual laser photodetachment suppression limits can be determined and the cooling of molecular anions into ground state explored. Other research questions to be addressed in the near future will be the application of the test results regarding the suppression of MgO^- to AMS measurements of ^{26}Al and furthermore the suppression of ^{36}S for measurements of ^{36}Cl.
Beside the 532 nm laser used for the experiments described in this thesis, also a tunable infrared laser with wavelengths from 1978 nm to 3002 nm and a maximum power of 6 W is already available. It will hopefully allow the suppression of ^{135}Ba for AMS measurements of ^{135}Cs [39, 40]. Furthermore the suppression of NiH with respect to FeH for measurements of ^{60}Fe, which is so far restricted to very large facilities, will be investigated.

A. SIMION 8.1 simulation files

A.1. Steerer geometry file

```
;steerer.gem -> SIMION 8.1 geometry for the x/y steerer
;AUTHOR: Tobias Moreau

;NOTES:
;electrode 1 : xplus
;electrode 2 : xplus_yminus
;electrode 3 : yminus
;electrode 4 : yminus_xminus
;electrode 5 : xminus
;electrode 6 : xminus_yplus
;electrode 7 : yplus
;electrode 8 : yplus_xplus

;grid density in grid units per millimeter can be changed here,
;PA definitions will be adjusted automatically.
# local grid_density = 5

;number of grid points in axial and radial direction, calculated
;from the grid density.
# local z_points = (101 * grid_density) + 1
# local xy_points = (104 * grid_density) + 1

;PA definitions depend on number of grid points in
;axial and radial direction and therefore on density
pa_define($(xy_points),$(xy_points),$(z_points),p,n,e,surface=fractional)

;main scaling factor, scales from grid units to millimeters
locate(,,,$(grid_density),,,){

e(0){
    fill{
    within{cylinder(52,52,1,52,52,1)}
        notin{cylinder(52,52,1.1,15,15,1.2)}
        within{cylinder(52,52,31,52,52,30)}
        notin{cylinder(52,52,31.1,50,50,30.2)}
        within{cylinder(52,52,101,52,52,30)}
        notin{cylinder(52,52,101.1,50,50,30.2)}
    }
```

```
}

e(1){
    locate(52,52,5,1,0,0,0){
        fill{
            within{box3d(-15.75,-44,0,15.75,-42,92)}
        }
    }
}

e(2){
    locate(52,52,5,1,0,45,0){
        fill{
            within{box3d(-15.75,-44,0,15.75,-42,92)}
        }
    }
}

e(3){
    locate(52,52,5,1,0,90,0){
        fill{
            within{box3d(-15.75,-44,0,15.75,-42,92)}
        }
    }
}

e(4){
    locate(52,52,5,1,0,135,0){
        fill{
            within{box3d(-15.75,-44,0,15.75,-42,92)}
        }
    }
}

e(5){
    locate(52,52,5,1,0,180,0){
        fill{
            within{box3d(-15.75,-44,0,15.75,-42,92)}
        }
    }
}

e(6){
    locate(52,52,5,1,0,225,0){
        fill{
            within{box3d(-15.75,-44,0,15.75,-42,92)}
        }
    }
```

```
}

e(7){
    locate(52,52,5,1,0,270,0){
        fill{
            within{box3d(-15.75,-44,0,15.75,-42,92)}
        }
    }
}

e(8){
    locate(52,52,5,1,0,315,0){
        fill{
            within{box3d(-15.75,-44,0,15.75,-42,92)}
        }
    }
}

}
```

A.2. Cooler geometry file

```
;ILIAS_cooler_geometry.gem -> SIMION 8.1 geometry for the entire ILIAS ion cooler section
;AUTHOR: Tobias Moreau

;NOTES:   - this geometry is scaled so that parameters have to be given in
;           millimeters instead of grid units.
;         - the geometry is based on gathered information from older simulations,
;           dimensions from construction plans and some directly measured lengths.
;           accuracy can't be guaranteed.
;         - the grid density can be easily changed (local variable 'grid_density'),
;           no need to rewrite the complete file.
;         - longitudinal positions of compontents are given relative to a
;           reference position (start of RF electrodes).
;         - the variables 'start_pos' and 'end_pos' define the longitudinal
;           simulation section. this makes it very easy to simulate only a certain
;           part of the whole geometry.
;         - to change the longitudinal position of e.g. a lens, normally only its
;           position variable has to be changed. these variables can be found at
;           the beginning of each electrode's section of code.
;         - be aware that conically shaped electrodes may be permeable (for ions) at
;           low grid densities (injection/extraction aperture, extraction lenses).

;fast adjustable electrodes:
;electrode 1 : injection high lens (INJHI)
;electrode 2 : injection low lens (INJLO)
;electrode 3 : entrance aperture
;electrode 4 : vertical RF electrodes
;electrode 5 : horizontal RF electrodes
;electrode 6 : guiding electrodes (GELEC)
;electrode 7 : exit aperture
;electrode 8 : extraction low lens (EXTLO)
;electrode 9 : extraction high lens (EXTHI)
;electrode 10: RFQ tube + cooler boundary

;grid density in grid units per mm can be changed here.
;PA definitions will be adjusted automatically.
# local grid_density = 4

;1546mm is the total longitudinal extent (z-direction) of the geometry.
;the simulated section goes from 'start_pos' to 'end_pos'. these positions are given in
;mm units, relative to the reference position (start of RF electrodes).
;start_pos = -298 and end_pos = 1248 would correspond to the complete geometry.
# local start_pos = -298  --from -298 to 1248
# local end_pos = 100      --from -298 to 1248

;number of grid points in axial and radial direction, calculated from the grid density:
# local z_points = ((end_pos-start_pos) * grid_density) + 1
```

```
# local xy_points = (76 * grid_density) + 1

;longitudinal reference position (start of RF electrodes) relative to which the
;z-positions of all components are specified. its position in the simulation grid changes
;with respect to the chosen geometry section.
# local ref_pos = -start_pos

;PA definitions depend on number of grid points in axial and radial direction and
;therefore on density.
pa_define($(xy_points),$(xy_points),$(z_points),p,xy,e,surface=fractional)

;main scaling factor, scales from grid units to mm:
locate(,,,$(grid_density),,,){
;========================================================================
;INJECTION HIGH LENS:

;position relative to the reference position of the surface closest to the reference
;position:
# local inj_hi_pos = ref_pos - 83.6

e(1){
    fill{
        locate(,,$(inj_hi_pos),1,,,){
            within{cylinder(,,,52.5,,1.5)}
            notin{cylinder(,,10,10,,21.5)}
        }
    }
}
;========================================================================
;INJECTION LOW LENS:

;16mm closest distance between the injection aperture and INJLO was estimated during the
;cooler opening in november 2014. in the original design it's 19mm.

;position of surface closest to the reference position:
# local inj_lo_pos = ref_pos - 23.1

e(2){
    fill{
        locate(,,$(inj_lo_pos),1,,,){
            within{cylinder(,,,35,,1.5)}
            notin{cylinder(,,10,5,,21.5)}
        }
    }
}
;========================================================================
;ENTRANCE APERTURE:
```

```
;corresponds to 0.1mm distance between RF-electrodes and aperture, which
;was estimated during cooler opening in November 2014.
;position of the surface furthest from the reference position.
# local inj_aperture_pos = ref_pos - 7.1
;for a distance of 1mm (original design) use:
;# local inj_aperture_pos = ref_pos - 8

e(3){
    ;align internal x-axis with external z-axis to draw sketch for rotate fill.
    ;internal origin located on non conical side of the aperture.
    locate(,,$(inj_aperture_pos),1,-90,,){
        rotate_fill(360){
            ;cone made thicker than in original aperture so that ions can't
            ;pass through at a grid density of 3gu/mm:
            within{polyline(0,8.3,0,25,2,25,2,8.64,7,1.5,6,1.5,0,8.3)}
            ;original design:
            ;within{polyline(0,8.3,0,25,2,25,2,8.64,7,1.5,6.8,1.5,0,8.3)}
            ;cut short cone to get a 6mm opening diameter:
            ;within{polyline(0,8.3,0,25,2,25,2,8.64,5.9496,3,4.6765,3,0,8.3)}
        }
    }
}
;======================================================================
;VERTICAL RF ELECTRODES:

# local vert_RF_elect_pos = ref_pos + 950

e(4){
    fill{
        within{cylinder(0,9.37,$(vert_RF_elect_pos),5,,950)}
    }
}
;======================================================================
;HORIZONTAL RF ELECTRODES:

;variable redundancy intended for the purpose of clarity.
# local horiz_RF_elect_pos = vert_RF_elect_pos

e(5){
    fill{
        within{cylinder(9.37,0,$(horiz_RF_elect_pos),5,,950)}
    }
}
;======================================================================
;GUIDING ELECTRODES:

# local guide_elect_pos = ref_pos
```

```
e(6){
    locate(,,$(guide_elect_pos),1,,-45,){
        ;last parameter in the following 'locate' line is the tilting angle.
        ;-0.036deg -> 1.2mm change in distance between opposite guide electrodes
        ;over electrode length (950mm).
        locate(0,6.18,0,1,0,0,-0.043){
            fill{
                within{cylinder(0,0.75,950,0.75,,950)}
                within{box3d(-0.75,0.75,0,0.75,7,950)}
            }
        }
    }
}
;======================================================================
;EXIT APERTURE:

;corresponds to 0.1mm distance between RF-electrodes and aperture, which
;was estimated during cooler opening in November 2014.
;position of the surface furthest from the reference position.
# local ext_aperture_pos = ref_pos + 957.1
;for a distance of 1mm (original design) use:
;# local ext_aperture_pos = ref_pos + 958

e(7){
    ;turn entrance aperture 180deg (Az: -90 -> 90)
    locate(,,$(ext_aperture_pos),1,90,0,0){
        rotate_fill(360){
            ;cone made thicker than in original aperture so that ions can't
            ;pass through at a grid density of 3gu/mm:
            within{polyline(0,8.3,0,25,2,25,2,8.64,7,1.5,6,1.5,0,8.3)}
            ;original design:
            ;within{polyline(0,8.3,0,25,2,25,2,8.64,7,1.5,6.8,1.5,0,8.3)}
        }
    }
}
;======================================================================
;EXTRACTION LOW LENS:

;16mm closest distance between the extraction aperture and the non conical part of EXTLO
;was estimated during the cooler opening in november 2014. in the original design it's
;19mm.

;position of non conical surface closest to the reference position:
# local ext_lo_pos = ref_pos + 976.1

e(8){
    locate(,,$(ext_lo_pos-5),1,-90,,){
        rotate_fill(360){
```

```
            ;cone made thicker so that ions can't pass through at a grid
            ;density of 3gu/mm:
            within{polyline(0,3.6,5,10.64,5,35,7,35,7,10.4,1,3.6,0,3.6)}
            ;original design:
            ;within{polyline(0,3.6,5,10.64,5,35,7,35,7,10.4,0.2,3.6,0,3.6)}
        }
    }
}
;=======================================================================
;EXTRACTION HIGH LENS:

;position of non conical surface closest to the reference position:
# local ext_hi_pos = ref_pos + 1037.1

e(9){
    locate(,,$(ext_hi_pos-18.5),1,-90,,){
        rotate_fill(360){
            within{polyline(0,10,20,30,20,52.5,18.5,52.5,18.5,31.06,0,12.12,0,10)}
        }
}
}
;=======================================================================
;RFQ TUBE + COOLER BOUNDARY:

;0.1mm distance between apertures and RF electrodes
# local RFQ_tube_pos = ref_pos + 954.1
# local cooler_boundary_pos = ref_pos - 104

;position variables for the boundaries of the INJLO and EXTLO lenses depend on lens
;positions -> when lens positions are changed, boundaries are adjusted automatically
# local inj_lo_boundary_pos = -1 * (cooler_boundary_pos - inj_lo_pos)
# local ext_lo_boundary_pos = (-1 * cooler_boundary_pos) + (ext_lo_pos-5) + 5

e(10){
    fill{
        locate(,,$(RFQ_tube_pos),1,,,){
            ;0.1mm distance between apertures and RF electrodes:
            within{cylinder(,,,25,,958.2)}
            ;for 1mm distance between apertures and RF electrodes use:
            ;within{cylinder(,,,25,,960)}
            notin{cylinder(,,10,20,,980)}
        }
    }
    locate(,,$(cooler_boundary_pos),1,-90,,){
        rotate_fill(360){
            within{box2d(0,75,1158,76)}
            within{box2d($(inj_lo_boundary_pos - 1.5),41,$(inj_lo_boundary_pos),75)}
            within{box2d($(ext_lo_boundary_pos),41,$(ext_lo_boundary_pos + 2),75)}
```

```
        }
    }
}
;======================================================================
;BEAMLINE OUTSIDE HIGH VOLTAGE REGION:

# local injection_beamline_pos = ref_pos - 298
# local extraction_beamline_pos = ref_pos + 1092

e(0){
    locate(,,$(injection_beamline_pos),1,-90,,){
        rotate_fill(360){
            within{box2d(0,75,156,76)}
            within{box2d(0,14.5,140.5,15.5)}
        }
    }
    locate(,,$(extraction_beamline_pos),1,-90,,){
        rotate_fill(360){
            within{box2d(0,75,156,76)}
            within{box2d(15.5,14.5,156,15.5)}
            within{polyline(5,5,6,5,15.5,14.5,15.5,15.5,5,5)}
        }
    }
}
;======================================================================
}
```

A.3. User program for the injection ion optics simulations

```
--injection_ion_optics.lua -> SIMION 8.1 workbench program for the injection ion optics
--simulations using the ILIAS_cooler_geometry.gem geometry.
--AUTHOR: Tobias Moreau

--[[DESCRIPTION:
    - sets RF voltage, randomizes ion time of birth, fast adjusts electrodes.
    - default RF parameters are set for 36Cl- ions.
    - counts ions transmitted into a defined circular region after each run.
    - displays counts and transmission of each run.
    - imports hard sphere collision model collision_hs1.lua from SIMION examples
      to simulate buffer gas.
    - if _simulation_mode == 1 user program is in lens voltage variation mode.
      this allows looping through INJHI and INJLO voltages, where the min and
      max voltage, as well as the increment can be chosen for each lens directly
      in the workbench window. the lens voltages and transmitted ion number of
      each run are written into the lens_variation_data.csv file.
    - if _simulation_mode == 2 the user program is in emittance measurement mode.
      a slightly modified version of emittance.lua from the SIMION examples is
      imported. ions splat on an xy plane for which the z position is chosen in
      the workbench window. the emittance is calculated for this position and
      displayed.
    - if _simulation_mode takes another value, simulations can be run without lens
      voltage looping and without emittance calculation.
]]
--=========================================================================
simion.workbench_program()
--=========================================================================
--import modified emittance calculation user program from SIMION examples:
local EMITT = simion.import ("emittance_modified.lua")
--import hard sphere collision model user program from SIMION examples:
local HS1 = simion.import ("collision_hs1.lua")
--=========================================================================
adjustable _cooler_HV = -29950  -- cooler high voltage [V]
adjustable _RF_freq = 2.6       -- frequency [MHz] (1/usec)
adjustable _RF_ampl = 200       -- RF amplitude [V] (relative to cooler HV)
adjustable _INJHI = 4000        -- INJHI lens voltage [V] (rel. to cooler HV)
adjustable _INJLO = 700         -- INJLO lens voltage [V] (rel. to cooler HV)
adjustable _inj_aperture = 0    -- voltage on injection aperture [V] (rel. to cooler HV)
adjustable _guide_elect = -50   -- guiding electrode voltage [V] (rel. to cooler HV)

local num_particles             -- number of flown ions
local num_cup_hits = 0          -- number of ions that splat in virtual Faraday cup
local trans                     -- transmission into  cup
adjustable _cup_pos = 393       -- z coordinate of cup position [mm]
adjustable _count_rad = 4.37    -- cup radius [mm]
```

```
adjustable _gas_start = 297.9   -- gas enabled from this z position on [mm]

-- 1 for lens variation mode, 2 for emittance mode, else for standard mode:
adjustable _simulation_mode = 1

--variables for lens voltage variation mode:
adjustable _INJHI_increment = 1000
adjustable _INJHI_min_volt = 0
adjustable _INJHI_max_volt = 12500
local INJHI_run_volt = 0

adjustable _INJLO_increment = 100
adjustable _INJLO_min_volt = 0
adjustable _INJLO_max_volt = 1250
local INJLO_run_volt = 0
--============================================================================
--results file initialization and clear up:
local results_file = assert(io.open("lens_variation_data.csv", "w"))  -- write mode ("w")
os.remove("lens_variation_data.csv")
--============================================================================
function segment.flym()
    if _simulation_mode == 1 then        -- reruns for different lens voltages
        for j = _INJHI_min_volt,_INJHI_max_volt,_INJHI_increment do
            for i = _INJLO_min_volt,_INJLO_max_volt,_INJLO_increment do
                INJHI_run_volt = j
                INJLO_run_volt = i
                run()
            end
        end
    else
        run()
        return
    end
    results_file:close()    -- closes tuning log file after termination of all runs
end
--===========================================================================
function segment.initialize_run()
    num_cup_hits = 0                -- reset the counter before each rerun
end
--===========================================================================
function segment.initialize()
    ion_time_of_birth = rand() / _RF_freq    -- randomizes ion time of birth
    if _simulation_mode ~= 2 then
        HS1.segment.initialize()
    end
end
--===========================================================================
function segment.init_p_values()
```

```
    if _simulation_mode == 1 then  -- lens variation mode lens voltages
        adj_elect01 = _cooler_HV + INJHI_run_volt
        adj_elect02 = _cooler_HV + INJLO_run_volt
    else -- regular mode lens voltages
        adj_elect01 = _cooler_HV + _INJHI
        adj_elect02 = _cooler_HV + _INJLO
    end
    adj_elect03 = _cooler_HV + _inj_aperture
    adj_elect06 = _cooler_HV + _guide_elect
    adj_elect10 = _cooler_HV
end
--============================================================================
function segment.tstep_adjust()
    if _simulation_mode ~= 2 then
        HS1.segment.tstep_adjust()
    end
end
--============================================================================
function segment.fast_adjust()
    --set RF voltage to RF electrodes:
    adj_elect04 = _cooler_HV + _RF_ampl * sin(ion_time_of_flight * 2 * math.pi * _RF_freq)
    adj_elect05 = _cooler_HV - _RF_ampl * sin(ion_time_of_flight * 2 * math.pi * _RF_freq)
end
--============================================================================
function segment.other_actions()
    if _simulation_mode == 2 then
        EMITT.segment.other_actions()
    else
        --disable gas for ions outside of RFQ tube:
        if ion_pz_mm < _gas_start or (ion_px_mm ^2+ion_py_mm ^2)^(1/2) > 25 then
            return
        end
        HS1.segment.other_actions()
    end
end
--============================================================================
function segment.terminate()
    num_particles = ion_number
    if _simulation_mode ~= 2 then
        -- count particles that splat within defined circular cup region:
if ion_pz_mm > _cup_pos and math.sqrt((ion_px_mm )^2 + (ion_py_mm )^2) <= _count_rad then
            num_cup_hits = num_cup_hits + 1
        end
    HS1.segment.terminate()
    end
end
--============================================================================
function segment.terminate_run()
```

```
    trans = 100 * num_cup_hits / num_particles
    if _simulation_mode == 1 then
        --print run data to workbench log window:
print('INJHI, INJLO, transmission = '..INJHI_run_volt..', '..INJLO_run_volt..', '..trans)
        -- write run data into lens_variation_data.csv:
        results_file:write(INJHI_run_volt..","..INJLO_run_volt..","..num_cup_hits.."\n")
        -- immediately output to disk:
        results_file:flush()
    elseif _simulation_mode == 2 then
        EMITT.segment.terminate_run()
    else
        print('ions in cup = ' ..num_cup_hits.. ' of '..num_particles)
        print('transmission = ' ..trans.. ' %')
    end
end
```

Bibliography

[1] R. Hellborg and G. Skog. Accelerator mass spectrometry. *Mass Spectrometry Reviews*, 27(5):398–427, 2008.

[2] A. E. Litherland, I. Tomski, X.-L. Zhao, L. M. Cousins, J. P. Doupé, G. Javahery, and W. E. Kieser. Isobar separation at very low energy for AMS. *Nuclear Instruments and Methods in Physics Research Section B: Beam Interactions with Materials and Atoms*, 259(1):230–235, 2007.

[3] W. Kutschera. Applications of accelerator mass spectrometry. *International Journal of Mass Spectrometry*, 349–350:203–218, 2013.

[4] W. Kutschera, P. Collon, H. Friedmann, R. Golser, P. Hille, A. Priller, W. Rom, P. Steier, S. Tagesen, A. Wallner, E. Wild, and G. Winkler. VERA: A new AMS facility in Vienna. *Nuclear Instruments and Methods in Physics Research Section B: Beam Interactions with Materials and Atoms*, 123(1–4):47–50, 1997.

[5] P. Steier, R. Golser, W. Kutschera, A. Priller, C. Vockenhuber, and S. Winkler. VERA, an AMS facility for "all" isotopes. *Nuclear Instruments and Methods in Physics Research Section B: Beam Interactions with Materials and Atoms*, 223–224:67–71, 2004.

[6] H.-A. Synal. Developments in accelerator mass spectrometry. *International Journal of Mass Spectrometry*, 349–350:192–202, 2013.

[7] C. Vockenhuber, M. Bichler, R. Golser, W. Kutschera, A. Priller, P. Steier, and S. Winkler. ^{182}Hf, a new isotope for AMS. *Nuclear Instruments and Methods in Physics Research Section B: Beam Interactions with Materials and Atoms*, 223–224:823–828, 2004.

[8] O. Forstner, H. Gnaser, R. Golser, D. Hanstorp, M. Martschini, A. Priller, J. Rohlén, P. Steier, C. Vockenhuber, and A. Wallner. Reassessment of ^{182}Hf AMS measurements at VERA. *Nuclear Instruments and Methods in Physics Research Section B: Beam Interactions with Materials and Atoms*, 269(24):3180–3182, 2011.

[9] J. Pitters. *Laser Photodetachment in a Gas-Filled RF-Quadrupole*. Master's thesis, University of Vienna, 2015.

[10] O. Forstner, P. Andersson, D. Hanstorp, J. Lahner, M. Martschini, J. Pitters, A.Priller, P. Steier, and R. Golser. The ILIAS project for selective isobar suppression by laser photodetachment. *Nuclear Instruments and Methods in Physics Research Section B: Beam Interactions with Materials and Atoms*, 361:217–221, 2015.

[11] O. Forstner, P. Andersson, C. Diehl, R. Golser, D. Hanstorp, W. Kutschera, A. Lindahl, A. Priller, P. Steier, and A. Wallner. Isobar suppression in AMS using laser photodetachment. *Nuclear Instruments and Methods in Physics Research Section B: Beam Interactions with Materials and Atoms*, 266(19–20):4565–4568, 2008.

[12] E. P. Wigner. On the Behavior of Cross Sections Near Thresholds. *Phys. Rev.*, 73:1002–1009, 1948.

[13] D. Berkovits, E. Boaretto, G. Hollos, W. Kutschera, R. Naaman, M. Paul, and Z. Vager. Selective suppression of negative ions by lasers. *Nuclear Instruments and Methods in Physics Research Section A: Accelerators, Spectrometers, Detectors and Associated Equipment*, 281(3):663–666, 1989.

[14] D. Berkovits, E. Boaretto, G. Hollos, W. Kutschera, R. Naaman, M. Paul, and Z. Vager. Study of laser interaction with negative ions. *Nuclear Instruments and Methods in Physics Research Section B: Beam Interactions with Materials and Atoms*, 52(3):378–383, 1990.

[15] T. Leopold, J. Rohlén, P. Andersson, C. Diehl, M. Eklund, O. Forstner, D. Hanstorp, H. Hultgren, P. Klason, A.O. Lindahl, and K. Wendt. Feasibility of photodetachment isobar suppression of WF_5^- with respect to HfF_5^-. *International Journal of Mass Spectrometry*, 359:12–18, 2014.

[16] Y. Liu, J. R. Beene, C. C. Havener, and J. F. Liang. Isobar suppression by photodetachment in a gas-filled rf quadrupole ion guide. *Applied Physics Letters*, 87(11), 2005.

[17] Y. Liu, J. F. Liang, G. D. Alton, J. R. Beene, Z. Zhou, and H. Wollnik. Collisional cooling of negative-ion beams. *Nuclear Instruments and Methods in Physics Research Section B: Beam Interactions with Materials and Atoms*, 187(1):117–131, 2002.

[18] Y. Liu, J.F. Liang, and J.R. Beene. A high efficiency RF quadrupole ion beam cooler for negative ions. *Nuclear Instruments and Methods in Physics Research Section B: Beam Interactions with Materials and Atoms*, 255(2):416–422, 2007.

[19] Y. Liu, P. Andersson, J. R. Beene, O. Forstner, A. Galindo-Uribarri, T. Gottwald, D. Hanstorp, C. C. Havener, A. O. Lindahl, and K. Wendt. Beam purification by photodetachment (invited). *Review of Scientific Instruments*, 83(2), 2012.

[20] P. H. Dawson. *Quadrupole mass spectrometry and its applications*. Elsevier Scientific Publishing Company, Amsterdam, 1976.

[21] W. Paul and H. Steinwedel. Notizen: Ein neues Massenspektrometer ohne Magnetfeld. *Zeitschrift für Naturforschung A*, 8(7):448–450, 1953. Retrieved 29 Apr. 2016, from doi:10.1515/zna-1953-0710.

[22] I. E. Dayton, F. C. Shoemaker, and R. F. Mozley. The Measurement of Two-Dimensional Fields. Part II: Study of a Quadrupole Magnet. *Review of Scientific Instruments*, 25(5):485–489, 1954.

[23] D. R. Denison. Operating Parameters of a Quadrupole in a Grounded Cylindrical Housing. *Journal of Vacuum Science & Technology*, 8(1):266–269, 1971.

[24] F. Herfurth, J. Dilling, A. Kellerbauer, G. Bollen, S. Henry, H.-J. Kluge, E. Lamour, D. Lunney, R. B. Moore, C. Scheidenberger, S. Schwarz, G. Sikler, and J. Szerypo. A linear radiofrequency ion trap for accumulation, bunching, and emittance improvement of radioactive ion beams. *Nuclear Instruments and Methods in Physics Research Section A: Accelerators, Spectrometers, Detectors and Associated Equipment*, 469(2):254–275, 2001.

[25] J. Lahner. *A neutral particle detector for phododetachment studies*. Master's thesis, University of Vienna, 2014.

[26] J. C. Rienstra-Kiracofe, G. S. Tschumper, H. F. Schaefer III, S. Nandi, , and G. B. Ellison. Atomic and Molecular Electron Affinities: Photoelectron Experiments and Theoretical Computations. *Chemical Reviews*, 102(1):231–282, 2002.

[27] K. Melber. *AMS-Messungen stabiler Platinisotope in präsolaren Nanodiamanten mit Hilfe eines neuen Negativ-Ionen-Injektors für VERA*. Doctoral thesis, University of Vienna, 2011.

[28] D. J. Manura and D. A. Dahl. *SIMION® Version 8.1.1.32*. Scientific Instrument Services, Inc., Ringoes, NJ 08551, 2013. http://simion.com/.

[29] J. R. Carmichael and D. J. Manura. *emittance.lua*. 2006. User program from SIMION® examples.

[30] A.E. Litherland. Accelerator mass spectrometry. *Nuclear Instruments and Methods in Physics Research Section B: Beam Interactions with Materials and Atoms*, 5(2):100–108, 1984.

[31] D. J. Manura. *collision_hs1.lua*. Scientific Instrument Services, Inc., 2005-06/2011. User program from SIMION® examples.

[32] R. Boussaid, G. Ban, and J. F. Cam. Experimental study of a high intensity radiofrequency cooler. *Phys. Rev. ST Accel. Beams*, 18:072802, 2015.

[33] T. Kim. *Buffer Gas Cooling of Ions in a Radio Frequency Quadrupole Ion Guide: A study of the cooling process and cooled beam properties.* Doctoral thesis, Department of Physics, McGill University, 1997.

[34] S. Schwarz. Simulations for Ion Traps - Buffer Gas Cooling. In *Trapped Charged Particles and Fundamental Interactions*, volume 749 of *Lect. Notes Phys.*, page 97–117. Springer-Verlag Berlin Heidelberg, 2008.

[35] S. Schwarz. IonCool - A versatile code to characterize gas-filled ion bunchers and coolers (not only) for nuclear physics applications. *Nuclear Instruments and Methods in Physics Research Section A: Accelerators, Spectrometers, Detectors and Associated Equipment*, 566(2):233–243, 2006.

[36] R. Middleton. *A Negative-Ion Cookbook.* Department Of Physics, University of Pennsylvania, Philadelphia, PA 19104, 1989 (Revised 1990).

[37] A. Arazi, T. Faestermann, J. O. Fernández Niello, D. Frischke, K. Knie, G. Korschinek, H. J. Maier, E. Richter, G. Rugel, and A. Wallner. Magnesium suppression for ^{26}Al measurements using AlO^- ions. *Nuclear Instruments and Methods in Physics Research Section B: Beam Interactions with Materials and Atoms*, 223–224:259–262, 2004.

[38] M. Gutowski, P. Skurski, X. Li, and L.-S. Wang. $(MgO)_n^-$ (n=1−5) Clusters: Multipole-Bound Anions and Photodetachment Spectroscopy. *Phys. Rev. Lett.*, 85:3145–3148, 2000.

[39] J. Lachner, M. Kasberger, M. Martschini, A. Priller, P. Steier, and R. Golser. Developments towards detection of ^{135}Cs at VERA. *Nuclear Instruments and Methods in Physics Research Section B: Beam Interactions with Materials and Atoms*, 361:440–444, 2015.

[40] M. Kasberger. *Accelerator mass spectrometry of cesium isotopes.* Diploma thesis, University of Vienna, 2015.

Abstract

The sensitivity of trace isotope measurements with accelerator mass spectrometry (AMS) is in many cases limited by the presence of stable isobars. They often cannot be removed or distinguished from the isotope under investigation by established methods. Therefore, isotopic ratios from 10^{-12} to 10^{-16} characteristic for AMS cannot be attained for many trace isotopes of potential interest.

At the Vienna Environmental Research Accelerator (VERA), an AMS-facility at the University of Vienna, a method for isobar suppression by laser photodetachment is being developed. It employs differences in the electron affinity of the trace isotope and its isobar to element-selectively neutralize the negative ions of the isobar. To that end, the ion beam is cooled to energies in the order of 0.1 eV in a buffer gas filled radio frequency quadrupole ion guide. This extends the laser-ion interaction time and thereby enables suppression of the isobaric beam part by many orders of magnitude.

For research and development purpose a test setup named ILIAS (Ion Laser InterAction Setup) was built. On the long run the system should be installed onto the injection site of VERA to improve present detection limits for trace isotopes.

The main aims of the thesis at hand were to develop the test setup into its final state and to characterize it using test isotopes. In the process the transmission through the ion cooler could be improved to over 60% and a photodetachment suppression of a $^{63}Cu^-$ test beam by more than five orders of magnitude could be shown. Furthermore, the residence time of the ions in the cooler was measured and the suppression of MgO^- relative to AlO^- explored. The latter could pave the way for a first application of this novel filtering technique in AMS measurements of ^{26}Al.

Zusammenfassung

Die Empfindlichkeit der Messung von Spurenisotopen mittels Beschleuniger-Massenspektrometrie (AMS) ist in vielen Fällen beschränkt durch vorhandene stabile Isobare. Diese können oftmals nicht mit etablierten Methoden abgetrennt bzw. vom untersuchten Isotop unterschieden werden. Aus diesem Grund ist es gegenwärtig noch nicht möglich, die für AMS charakteristischen Isotopenverhältnisse von 10^{-12} bis 10^{-16} für viele potentiell interessante Spurenistope zu erreichen.
Am Vienna Environmental Research Accelerator (VERA), einer AMS-Anlage der Universität Wien, wird derzeit eine Methode zur Isobarenunterdrückung mittels Laser-Photodetachment entwickelt. Diese nutzt Unterschiede in der Elektronenaffinität von Spurenisotop und Isobar, um die negativen Ionen des Isobars mit einem Laser elementselektiv zu neutralisieren. Dazu wird der Ionenstrahl in einem mit Puffergas gefüllten Radiofrequenz-Quadrupol-Ionenkühler temporär auf Energien in der Größenordnung von 0.1 eV gebremst, um die Laser-Ionen-Wechselwirkungszeit zu verlängern und somit den störenden Isobarenanteil des Strahls um viele Größenordnungen unterdrücken zu können.
Für Forschungs- und Entwicklungszwecke wurde ein Testaufbau namens ILIAS (Ion Laser InterAction Setup) errichtet. Auf lange Sicht soll das System in die Niederenergieseite von VERA integriert werden, um bestehende Nachweisgrenzen bei der Messung von Spurenisotopen zu verbessern.
Die vorliegende Arbeit hatte primär zum Ziel, den Testaufbau in seine letztendliche Form zu bringen und mit Testisotopen zu charakterisieren. Es gelang dabei die Transmission durch den Ionenkühler auf über 60% zu verbessern. In Testexperimenten konnte auch eine Unterdrückung eines $^{63}Cu^-$ Strahls von über fünf Größenordnungen durch Laser-Photodetachment gezeigt werden. Weiters wurde die Aufenthaltsdauer im Kühler gemessen und die Unterdrückung von MgO^- gegenüber AlO^- untersucht. Letzteres könnte bei AMS-Messungen von ^{26}Al zu einer der ersten Anwendungen dieser neuentwickelten Filtermethode führen.